# MATERNAL MICRORNAS AND THE PLACENTAL RESPONSE TO ALCOHOL

A Dissertation

by

ALEXANDER MIKE TSENG

Submitted to the Office of Graduate and Professional Studies of
Texas A&M University
in partial fulfillment of the requirements for the degree of

DOCTOR OF PHILOSOPHY

| | |
|---|---|
| Chair of Committee, | Rajesh C. Miranda |
| Committee Members, | Darwin J. Prockop |
| | Ken Muneoka |
| | Stephen H. Safe |
| Head of Program, | Carol Vargas-Bautista |

May 2021

Major Subject: Medical Sciences

Copyright 2021 Alexander Mike Tseng

# ABSTRACT

Prenatal Alcohol exposure (PAE), like other pregnancy complications, can result in placental insufficiency and fetal growth restriction, though the linking causal mechanisms are unclear. We previously identified 11 gestationally-elevated maternal circulating miRNAs that predicted infant growth deficits following PAE. Here, we investigated whether these $_{HEa}$miRNAs contribute to the pathology of PAE, by inhibiting trophoblast epithelial-mesenchymal transition (EMT), a pathway critical for placental development. We now report for the first time, that PAE inhibits expression of placental pro-EMT pathway members in both rodents and primates, and that $_{HEa}$miRNAs collectively, but not individually, mediate placental EMT inhibition. $_{HEa}$miRNAs collectively, but not individually, also inhibited cell proliferation and the EMT pathway in cultured trophoblasts, while inducing cell stress, and following trophoblast syncytialization, aberrant endocrine maturation. Moreover, a single intra-vascular administration of the pooled murine-expressed $_{HEa}$miRNAs, to pregnant mice, decreased placental and fetal growth, reduced placentally directed blood flow, and inhibited expression of pro-EMT transcripts in placenta. Our data suggests that $_{HEa}$miRNAs collectively interfere with placental development, contributing to the pathology of PAE, and perhaps also, to other causes of fetal growth restriction.

# DEDICATION

This dissertation is dedicated to colleagues, family, and friends through which all things are possible.

# ACKNOWLEDGEMENTS

I would like to thank my committee chair, Dr. Miranda, and my committee members, Dr. Prockop, Dr. Muneoka, and Dr. Safe for their guidance and support throughout the course of this research.

Thanks also go to my friends and colleagues and the department faculty and staff for making my time at Texas A&M University a great experience. Finally, thanks to my family and friends for their encouragement.

## CONTRIBUTORS AND FUNDING SOURCES

This work was supervised by a dissertation committee consisting of Professor Rajesh C. Miranda [advisor], Professor Darwin J. Prockop of the Department of Institute for Regenerative Medicine, Professor Ken Muneoka of the Department of Veterinary Physiology and Pharmacology and Professor Stephen Safe of the Department of Veterinary Physiology and Pharmacology.

Human studies and accompanying multivariate statistical modelling in section 3.2 was performed in assistance with Alan Wells and Dr. Christina Chambers of the University of California San Diego. Non-human primate placental RNA used in section 3.4 was provided by Natali Newman, Nicole A.R. Walter, Dr. Victoria Roberts, and Dr. Christopher Kroenke of the Oregon National Primate Research Center. Rat placental tissue used in section 3.4 was generously provided by Drs. Lisa K. Akison and Karen M. Moritz from the University of Queensland. Mouse placental tissue used in chapter 3.4 was sourced from Dr. Andrea Allan from the University of New Mexico. Calcium imaging reported in chapter 3.12 was performed in collaboration with Dr. Amanda Mahnke of the Department of Neuroscience and Experimental Therapeutics. All other work conducted for the dissertation was completed by the student independently.

Graduate study was supported by the Doctoral Merit Fellowship from Texas A&M University and a predoctoral fellowship F31 AA026505 from the National Institute of Health (NIH). Its contents are solely the responsibility of the authors and do not necessarily represent the official views of the NIH or Texas A&M University.

# NOMENCLATURE

| | |
|---|---|
| 7AAD | 7-Aminoactinomycin D |
| ANOVA | Analysis of Variance |
| ATP | Adenosine Triphosphate |
| CIFASD | Collaborative Initiative on Fetal Alcohol Spectrum Disorders |
| ECAR | Extracellular Acidification Rate |
| EdU | 5-Ethynyl-2'-deoxyuridine |
| EMT | Epithelial-Mesenchymal Transition |
| FAS | Fetal Alcohol Syndrome |
| FASD | Fetal Alcohol Spectrum Disorders |
| FCS | Fetal Calf Serum |
| hCG | Human Chorionic Gonadotropin |
| HEa | Heavily Exposed Affected |
| HEua | Heavily Exposed Unaffected |
| HSD | Tukey’s Honest Significance Difference |
| IACUC | Institutional Animal Care and Use Committee |
| MANOVA | Multivariate Analysis of Variance |
| miRNA | microRNA |
| OCR | Oxygen Consumption Rate |
| ONPRC | Oregon National Primate Research Center |
| PAE | Prenatal Alcohol Exposure |

| | |
|---|---|
| UE | Unexposed |

TABLE OF CONTENTS

Page

LIST OF FIGURES

LIST OF TABLES

TABLE Page

# 1. INTRODUCTION[*]

Alcohol use during pregnancy remains prevalent despite published prevention guidelines (1). A recent meta-analysis determined the global prevalence of alcohol use during pregnancy at 9.8% (2). Within the United States, a 2013 study found 18% of women reported alcohol consumption during pregnancy, and 6.6% engaged in binge-drinking episodes, which are particularly damaging to fetal development (3). In the state of Texas, we recently reported an average state-wide third-trimester rate of alcohol exposure of 8.4%, with rates as high as 17.7% in some localities (4). These data collectively suggest that prenatal alcohol exposure (PAE) is common.

PAE harms the developing embryo and fetus and can result in a constellation of adverse infant outcomes, including craniofacial dysmorphologies, growth retardation, and neurobehavioral abnormalities, collectively termed Fetal Alcohol Spectrum Disorders (FASDs) (5). Estimates for the prevalence of FASDs range from 2-5% of the school age population in the US and Western Europe (6) to 13.6-20.9% in South Africa (7). Estimates for the global prevalence of fetal alcohol syndrome (FAS), the most severe end of the FASD continuum, characterized by cranio-facial dysmorphologies, growth restriction, and CNS abnormalities, range from 0.15 to 0.3% (8, 9), but are much higher in specific populations, for example, as high as 5.9-9.1% in the Cape Coloured (mixed ancestry) community in South Africa (7).

Given the lifelong debility and economic burden associated with FASDs (10),

[*] Part of this chapter is reprinted with permission from "Maternal circulating miRNAs that predict infant FASD outcomes influence placental maturation" by Tseng et al., 2019. *Life Science Alliance*, Vol. 2, © 2019 by Tseng et al.

there is an urgent need to develop sensitive and specific methodologies to identify affected children early in development, as well as develop interventions which can mitigate the effects of PAE on the developing fetus. In 2016, we reported that elevated levels of 11 distinct microRNAs (miRNAs) in 2nd and 3rd trimester maternal circulation distinguished infants who were affected by in-utero alcohol exposure (Heavily Exposed Affected: HEa) from those who were apparently unaffected at birth by PAE (Heavily Exposed Unaffected: HEua), or those who were unexposed (UE) (11) . We predicted that these $_{HEa}$miRNAs (MIMAT0004569 [hsa-miR-222-5p], MIMAT0004561 [hsa-miR-187-5p], MIMAT0000687 [hsa-mir-299-3p], MIMAT0004765 [hsa-miR-491-3p], MIMAT0004948 [hsa-miR-885-3p], MIMAT0002842 [hsa-miR-518f-3p], MIMAT0004957 [hsa-miR-760], MIMAT0003880 [hsa-miR-671-5p], MIMAT0001541 [hsa-miR-449a], MIMAT0000265 [hsa-miR-204-5p], MIMAT0002869 [has-miR-519a-3p]) in addition to being biomarkers of infant outcome following PAE, influence signaling pathways crucial for early development, particularly the epithelial-mesenchymal transition (EMT) pathway (11).

Placental development involves maturation of the cytotrophoblasts at the tip of anchoring villi into invasive extravillous trophoblasts, as well as fusion of cytotrophoblasts into multinucleate, hormone-producing syncytiotrophoblasts (12). Maturation into extravillous trophoblasts, which invade the maternal decidua and remodel the uterine spiral arteries into low-resistance high-flow vessels that enable optimal perfusion for nutrient and waste exchange, requires cytotrophoblasts to undergo EMT (13). Impaired placental EMT, as well as orchestration of the opposing

mesenchymal-epithelial transition pathway, has been found in conditions resulting from placental malfunction, primarily preeclampsia (14-19). While there have been no previous studies directly investigating the effects of PAE on placental EMT, a rodent study demonstrated that PAE, during a broad developmental window, reduced the number of invasive trophoblasts within the mesometrial triangle, a region of the uterine horn directly underlying the decidua (20). Furthermore, both human and rodent studies have found PAE disrupts placental morphology, and interferes with cytotrophoblast maturation, as with preeclampsia (21-24). Disrupted trophoblast maturation, seen in these conditions, is associated with aberrant expression of placental hormones, primarily human chorionic gonadotropin (hCG) (25-28). Our study is the first to report that PAE interferes with expression of core placental EMT pathway members. We also provide evidence that a group of circulating maternal miRNAs, $_{HEa}$miRNAs, which predict adverse infant outcomes due to PAE, mediate some of PAE's effects and interfere with EMT and cytotrophoblast maturation.

# 2. MATERIALS AND METHODS*

## 2.1 Mouse model of PAE

C57/BL6J mice (Jackson Laboratory, Bar Harbor, ME) were housed under reverse 12-hour dark / 12-hour light cycle (lights off at 08:00 hours). PAE was performed using a previously described limited access paradigm of maternal drinking (118, 119). Briefly, 60-day old female mice were subjected to a ramp-up period with 0.066% saccharin containing 0% ethanol (2 days), 5% ethanol (2 days), and finally 10% ethanol for 4-hours daily from 10:00–14:00 beginning 2 weeks prior to pregnancy, continuing through gestation (Figure 1A). Female mice offered 0.066% saccharin without ethanol during the same time-period throughout pregnancy served as controls. Tissue from the labyrinth, junctional, and decidual zone of male and female gestational day 14 (GD14) placentae were microdissected, snap-frozen in liquid nitrogen, and stored at -80$^{a}$C preceding RNA and protein isolation.

## 2.2 Mouse model for $_{HEa}$miRNA overexpression

For systemic administration of miRNAs, previously nulliparous C57/BL6NHsd dams (Envigo, Houston, TX) were tail-vein-injected on GD10 with either 50 μg of miRNA miRVana$^{TM}$ mimic negative control (Thermo Fisher, Waltham, MA, Cat No. 4464061) or pooled $_{HEa}$miRNA miRVana$^{TM}$ mimics in In-vivo RNA-LANCEr II (Bioo Scientific, Austin, TX, 3410-01), according to manufacturer instructions. The 50 μg of pooled $_{HEa}$miRNA mimics consisted of equimolar quantities of mmu-miR-222-5p, mmu-

* Part of this chapter is reprinted with permission from "Maternal circulating miRNAs that predict infant FASD outcomes influence placental maturation" by Tseng et al., 2019. *Life Science Alliance*, Vol. 2, © 2019 by Tseng et al.

miR-187-5p, mmu-mir-299a, mmu-miR-491-3p, miR-760-3p, mmu-miR-671-3p, mmu-miR-449a-5p, and mmu-miR-204-5p mimics. For bio-distribution studies, 50 μg of pooled equimolar quantities of hsa-miR-519a-3p and hsa-miR-518f-3p mimics were injected via tail vein. These human miRNAs were selected because no mouse homologs are known to exist and consequently, estimates for organ distribution of exogenous miRNAs in the mouse are unlikely to be contaminated by the expression of endogenous murine miRNAs. GD10 is a time point near the beginning of the developmental period of branching morphogenesis, immediately following chorioallantoic attachment, during which the placenta invades the maternal endometrium (120). At GD18, pregnancies were terminated with subsequent quantification of fetal weight, crown-rump length, snout-occipital distance, biparietal diameter, and placental weight. Subsequently, tissue was snap-frozen in liquid nitrogen, and stored at -80$^{a}$C preceding RNA isolation.

**2.3 Rat model of PAE**

Outbred nulliparous Sprague-Dawley rats were housed under a 12-hour light/12-hourdark cycle. PAE in Sprague-Dawley was conducted according to our previously published exposure paradigm (23, 121). Briefly, dams were given a liquid diet containing either 0% or 12.5% ethanol (vol/vol) from 4 days prior to mating until GD4 (Figure 1B). Dams had *ad libitum* access to the liquid diet 21-hours daily and consumed equivalent calories. Water offered during the remaining 3-hours of the day. On GD5, liquid diets were removed and replaced with standard laboratory chow. On GD20, placentas were immediately separated into the labyrinth and junctional zone, snap frozen in liquid nitrogen and stored at −80 °C preceding RNA isolation.

## 2.4 Non-human primate model of PAE

As previously described in detail (91), adult female rhesus macaques were trained to orally self-administer either 1.5 g/kg/d of 4% ethanol solution (equivalent to 6 drinks/day), or an isocaloric control fluid prior to time-mated breeding. Each pregnant animal continued ethanol exposure until gestational day 60 (GD60, term gestation is 168 days in the rhesus macaque) (122). Pregnancies were terminated by cesarean section delivery at three different time points; GD85, GD110, or GD135 (Figure 1C). The macaque placenta is typically bi-lobed with the umbilical cord insertion in the primary lobe and bridging vessels supplying the fetal side vasculature to the secondary lobe (Figure 4D showing gross placenta anatomy) (123) . Full thickness tissue biopsies (maternal decidua to fetal membranes) were taken from both the primary and secondary lobes of the placenta (Figure 4D showing H&E section of placenta). Samples were immediately snap-frozen in liquid nitrogen and stored at -80$^{o}$C preceding RNA isolation.

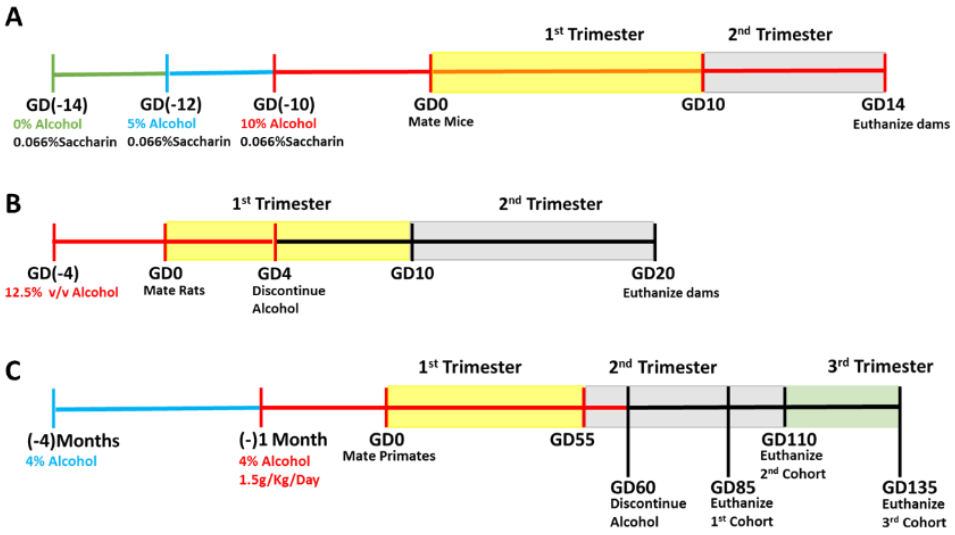


**Figure 1: PAE paradigms in mouse, rat, and macaques**
**A)** Timeline of mouse alcohol administration
**B)** Timeline of rat alcohol administration
**C)** Timeline of macaque alcohol administration

## 2.5 Characterization of fetal blood flow dynamics

Ultrasound imaging was conducted as previously described. Briefly, dams were anesthetized using isoflurane (anesthesia was initiated with 3–4% isoflurane and maintained with 1% isoflurane). Dams were maintained in the supine position on a temperature-controlled platform (with sensors for monitoring of maternal electrocardiogram, respiration and core body temperature, Visualsonics, Toronto, Canada). Prior to imaging, the abdomen was depilated (using Nair) to improve contact with the transducer and ultrasound gel applied. For each pregnant dam, a fetus in the upper left and upper right quadrant of the uterine horn were selected for repeated imaging on GD12, GD14, and GD18. Color and pulse wave Doppler measurements for umbilical arteries and ascending aorta were obtained using a high-frequency VEVO2100

ultrasound imaging machine coupled to a MS550D Microscan™ transducer with a center frequency of 40MHz (Visualsonics, Canada).

**2.6 Cell culture trophoblast models**

BeWO human cytotrophoblastic choriocarcinoma cells and HTR-8/SVneo extravillous cells were sourced from ATCC (Manassas, VA, Cat No. CCL-98 and CRL-3271 respectively). BeWO cells were maintained in HAM's F12 media containing penicillin (100 U/ml), streptomycin (100 μg/ml), and 10% vol/vol fetal calf serum (FCS) at 37°C and 5% $CO_2$. HTR8 cells were maintained in RPMI-1640 media with 5% vol/vol FCS, under otherwise identical conditions. Culture medium was replenished every 2 days and cells sub-cultured every 4-5 days.

BeWO cells were treated with 20 μm forskolin to induce syncytialization, as previously described (124, 125). BeWO and HTR8 cells were also subjected to four separate ethanol treatment conditions: 0 mg/dL, 60 mg/dl (13 mM),120 mg/dl (26 mM) or 320 mg/dl (70 mM). To achieve $_{HEa}$miRNA overexpression and inhibition, Dharmacon miRIDIAN$^{TM}$ miRNA mimics and hairpin inhibitors [25 nM], or control mimic (Dharmacon, Lafeyette CO, Cat No. CN-001000-01-05) and hairpin inhibitor (Dharmacon, Cat No. CN-001000-01-05) [25nm], were transfected into subconfluent BeWO and HTR8 cells using RNAIMAX lipofection reagent (Thermo Fisher, Cat No. 13778).

**2.7 Cell cycle analysis**

At 48-hours-post transfection, BeWO cells were pulsed with 10 μM EdU for 1-hour. Cells were immediately harvested, and cell cycle analysis was performed with the

Click-iT® EdU Alexa Fluor® 488 Flow Cytometry Assay Kit (Thermo Fisher, Cat No. C10420), in conjunction with 7AAD (Thermo Fisher, Cat No. 00-6993-50), according to manufacturer instructions, using the Beckman Coulter® Gallios 2/5/3 Flow Cytometer. Data was analyzed using Kaluza software (Beckman Coulter, Brea, CA).

**2.8 Cell death analysis**

BeWO cell culture was harvested 48-hours post transfection media was subjected to lactate dehydrogenase (LDH) detection using the Pierce™ LDH Cytotoxicity Assay Kit (Thermo Fisher, Cat No. 88953), according to manufacturer instructions, for lytic cell death quantification. The Promega Caspase-Glo® 3/7 Assay Systems (Promega, Madison, WI, Cat No. G8091) was used to quantify apoptotic cell death

**2.9 Invasion assay**

At 24-hours post-transfection and/or ethanol exposure, HTR8 cells were serum starved for an additional 18-hours. Subsequently, HTR8 cells were seeded onto trans-well permeable supports precoated with 300 µg/mL Matrigel (Corning, Corning, NY, Cat No. 354248). After 24-hours, cells remaining in the apical chamber were removed with a cotton swab. Cells that invaded into the basal chamber were incubated with 1.2 mM 3-(4,5-dimethylthiazol-2-yl)-2,5-diphenyltetrazolium bromide (MTT) for 3-hours, and the precipitate solubilized with 10% sodium dodecyl sulfate in 0.01N hydrochloric acid. Absorbance intensities were read at 570 nm in a Tecan Infinite® 200 plate reader.

**2.10 Metabolic flux analysis and calcium imaging**

BeWO cells (10,000/well) were plated into Seahorse XF96 Cell Culture Microplates (Agilent Biotechnology, Cat No. 103275-100). The oxygen consumption

rate (OCR), a measure of mitochondrial respiration, and extracellular acidification rate (ECAR), a measure of glycolysis, were measured using the Seahorse XFe96 flux analyzer (Seahorse Bioscience, North Billerica, MA). At the time of assay, cell culture medium was replaced with the appropriate pre-warmed Seahorse XF Base Medium (Agilent Biotechnology, Santa Clara, CA, Cat No. 102353-100). OCR and ECAR parameters were measured using the Seahorse XFp Cell Energy Phenotype Test Kit™ (Agilent Biotechnology, Cat No. 103275-100). Metabolic stress was induced by simultaneous treatment with 1μm Oligomycin and 0.125μM Carbonyl cyanide p-[trifluoromethoxy]-phenyl-hydrazone (FCCP).

BeWO cells were also plated onto glass coverslips in 24 well plates at a density of 30,000 cells/well. After exposure to ethanol and/or forskolin in culture, cells were prepared for calcium imaging. After replacement of culture media with external imaging media (154 mM NaCl, 5 mM KCl, 2 mM $CaCl_2$, 0.5 mM $MgCl_2$, 5 mM glucose, 10 mM HEPES, pH 7.4), cells were loaded for 35 minutes at 37°C with the calcium indicator dye fluo-4 AM (Thermo Fisher Scientific, Cat No. F14201), at a final concentration of 5μM fluo-4 AM in 0.1% DMSO. After incubation, cells were washed to remove remaining extracellular fluo-4 and imaged at 40x using confocal microscopy (FV1200-equipped BX61WI microscope, Olympus Corporation, Center Valley, PA). Time-lapse images were acquired at a frequency of 0.5Hz. Individual cells were manually outlined, and area and mean fluorescence intensity were obtained for each cell (FIJI image processing package)(126) . To determine the functional calcium range of each cell, at the end of imaging, cells were exposed to 5 μM ionomycin and 10 mM EGTA (0mM

external $Ca^{2+}$, $F_{range} = F_{ionomycin} - F_{EGTA}$). Baseline fluorescence was determined by averaging the lowest 5 consecutive fluorescence values during the initial 5 minutes ($F_{baseline}$) which was then expressed as a percentage of $F_{range}$ ($\Delta F_{baseline} = (F_{baseline} - F_{EGTA})/F_{range}$ X100). Maximal intracellular calcium response to 100 µM ATP was determined by averaging the highest 3 consecutive fluorescence values during ATP application ($F_{ATP}$) and determining the amount of fluorescence as a percentage of $F_{range}$ ($\Delta F_{ATP} = (F_{ATP} - F_{EGTA})/F_{range}$ X100).

**2.11 Quantitative reverse transcriptase-polymerase chain reaction (qRT-PCR) analysis**

Total RNA was extracted from tissue, well as BeWO and HTR8 cells, using the miRNeasy Mini kit (Qiagen, Cat No. 217004). For miRNA qPCR assays, cDNA was synthesized from 200 ng of total RNA using the miRCURY LNA Universal RT cDNA synthesis kit (Exiqon, Cat No. 203301/Qiagen, Cat No. 339340, Germantown, MD) and expression was assessed using miRCURY LNA SYBR Green (Exiqon, Cat No. 203401/Qiagen, Cat No. 339345). For mRNA qPCR assays, cDNA was synthesized from 500 ng of total RNA using the qScript™ cDNA Synthesis Kit (Quanta/Qiagen, Cat No. 95047). Gene expression analysis was performed using PerfeCTa SYBR Green FastMix (Quanta, Cat No. 95073) on the ViiA 7 Real-Time PCR System (Thermo Fisher Scientific). The data presented correspond to the mean $2^{-\Delta\Delta Ct}$ after being normalized to the geometric mean of β-actin, HPRT1, and 18s rRNA. Expression data for miRNA was normalized to the geometric mean of miR-25-3p, miR-574-3p, miR-30b-5p, miR-652-3p, and miR-15b-5p. For each primer pair, thermal stability curves were assessed for

evidence of a single amplicon and the length of each amplicon was verified using agarose gel electrophoresis. A list of primers and their sequences is presented in Table 1.

**2.12 Western immunoblotting analysis**

Protein was extracted using 1X RIPA lysis buffer (Millipore Sigma, Burlington MA) supplemented with Halt protease inhibitor cocktail (Thermo Fisher Scientific). Tissue was homogenized using the Branson Sonifier 150. Protein concentration was determined using Pierce BCA protein assay kit (Thermo Fisher Scientific) and 30 μg of protein was loaded onto a 4-12% Bis-Tris (Invitrogen/Thermo Fisher Scientific, Cat No. NPO323BOX), size fractionated at 200 V for 35 minutes, and transferred to a PVDF membrane using the iBlot transfer system (Invitrogen/Thermo Fisher Scientific). Blots with protein from cultured cells were blocked with 5% nonfat dry milk in tris-buffered saline containing Tween®-20 (TTBS) for 1-hour and incubated overnight with primary antibody. The blot was then washed and incubated with an HRP-conjugated goat anti-rabbit or anti-mouse IgG (Invitrogen) at dilution 1:1000 for 1-hour, then developed using PerkinElmer Western Lightning Plus Chemi ECL (PerkinElmer; Waltham, MA) and visualized using a CCD camera (Fluorchem Q, Alpha Innotech; San Leandro, CA). Blots with protein from homogenized tissue were dried overnight, rehydrated in methanol, stained with REVERT™ Total Protein Stain and developed with the Odyssey CLx Imaging System (LI-COR, Lincoln, NE). Blots were then blocked with Odyssey® Blocking Buffer (TBS) for 1h and incubated overnight with primary antibody. The blot was then washed and incubated with IRDye® 800CW secondary antibody (LI-COR, Cat No. 925-32210). The following antibodies were used: β-Actin HRP (Santa Cruz

Biotechnology, Cat No. sc-47778); Goat anti-Mouse IgG (H+L) Secondary Antibody, HRP (Thermo Fisher, Cat No. 62-6520); Goat anti-Rabbit IgG (H+L) Secondary Antibody, HRP (Thermo Fisher, Cat No. 65-6120); purified Mouse Anti-E-cadherin (BD Biosciences, Cat No. 610181), Rabbit anti-vimentin antibody [EPR3776] (Abcam, Cat No. ab 924647). Protein levels were quantified using the densitometric analysis package in FIJI image processing software (126).

**2.13 ELISA**

The 2nd and 3rd trimester maternal plasma samples were collected as part of a longitudinal cohort study conducted in two regions of Western Ukraine as part of the Collaborative Initiative on Fetal Alcohol Spectrum Disorders (CIFASD.org) between the years 2006 and 2011, as previously reported(11). Plasma, at a 1:1000 dilution, was subjected to hCG detection using Abcam's intact human hCG ELISA kit (Cat no. ab100533) following the manufacturer's protocol.

**2.14 Literature review**

We conducted a literature review for $_{HEa}$miRNAs and their associated gestational pathology using the National Institute of Health's Pubmed search interface. For each miRNA, the following search parameters were used:

*[miRX OR miR X OR miRNA X OR miRNAX or miRNX] AND MeSH Term*

where X represents the miRNA of interest and automatic term expansion was enabled. The following MeSH terms, and related search terms (in brackets), were used: Fetal Growth Retardation [Intrauterine Growth Retardation, IUGR Intrauterine Growth Restriction, Low Birth Weight, LBW, Small For Gestational Age, SGA], Premature

Birth [Preterm Birth, Preterm Birth, Preterm Infant, Premature Infant, Preterm Labor, Premature Labor], Spontaneous Abortion [Early Pregnancy Loss, Miscarriage, Abortion, Tubal Abortion, Aborted Fetus], Pre-Eclampsia [Pre Eclampsia, Preeclampsia, Pregnancy Toxemia, Gestational Hypertension, Maternal Hypertension], and Maternal Exposure [Environmental Exposure, Prenatal Exposure]. Returned articles were subsequently assessed for relevance.

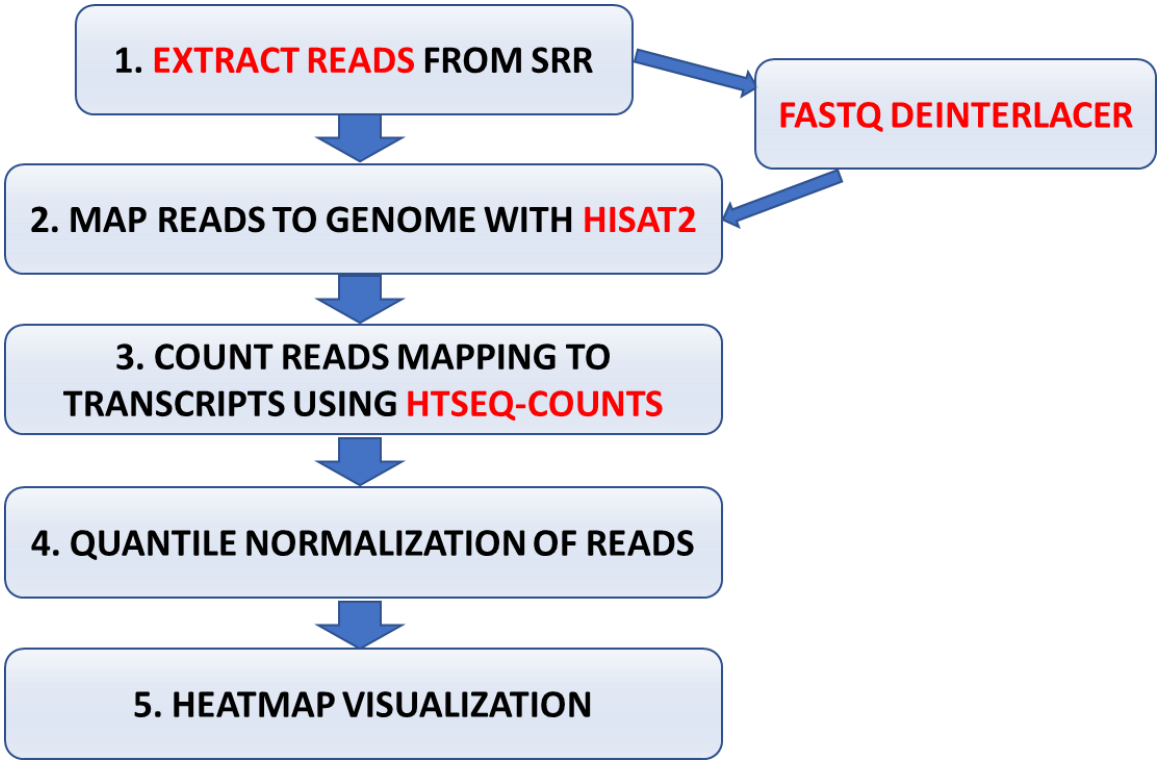


**Figure 2: Bioinformatics pipeline used to analyze $_{HEa}$miRNA pri-miRNA expression in tissues.**

### 2.15 Secondary analysis of RNA sequencing data

Expression levels of $_{HEa}$miRNAs in tissues were determined using the Human miRNA Expression Database and the miRmine Human miRNA expression database(66, 127). For expression analysis of $_{HEa}$miRNA pri-miRNAs, RNA sequencing data was

used from NCBI's sequence read archive (https://www.ncbi.nlm.nih.gov/sra). The accession numbers for the sequence files are: uterus (SRR1957209), thyroid (SRR1957207), thymus (SRR1957206), stomach (SRR1957205), spleen (SRR1957203), small intestine (SRR1957202), skeletal muscle (SRR1957201), salivary gland (SRR1957200), placenta (SRR1957197), lung (SRR1957195), liver (SRR1957193), kidney (SRR1957192), heart (SRR1957191), whole brain (SRR1957183), adrenal gland (SRR1957124), bone marrow (ERR315396), colon (ERR315484), adipose tissue (ERR315332), and pancreas (ERR315479). Deep sequencing analysis was conducted using the Galaxy version 15.07 user interface according to the bioinformatics pipeline outlined in Figure 2.

**2.16 Statistical analyses**

Linear regression models were used to estimate associations between infant growth measures and miRNA expression levels, gestational age at blood draw, the interaction between subject-centered miRNA expression level and gestational age at blood draw, and child sex. Spearman correlations between infant growth measures and subject-centered miRNA expression levels were also calculated. Linear regression models were also used to estimate the associations between gestational at birth and log-transformed hCG levels, ethanol intake, the interaction between log-transformed hCG levels and ethanol intake, gestational at blood draw, and child sex. Statistical Analysis and graphs were generated with GraphPad Prism 6 software (GraphPad Software, Inc., La Jolla, CA), SPSS v24, or R version 3.3.1. Results are expressed as the mean ± SEM, or alternatively as box-and-whisker plots with the bounds of the box demarcating limits

of 1st and 3rd quartile, a median line in the center of the box, and whiskers representing the total range of data. The overall group effect was analyzed for significance using 1-way MANOVA, 1-way or 2-way ANOVA with Tukey's Honest Significance Difference (HSD) post-hoc testing when appropriate (i.e. following a significant group effect in 1-way ANOVA or given a significant interaction effect between experimental conditions in 2-way ANOVA), to correct for a family-wise error rate. A 2-tailed Student's t-test was used for planned comparisons. For experiments characterizing the individual effects of $_{HEa}$miRNAs against the control miRNA or antagomirs, individual 2-tailed Student's t-test with 5% FDR correction was applied to account for multiple comparisons. All statistical tests, sample-sizes, and post-hoc analysis are appropriately reported in the results section. A value of $p < 0.05$ was considered statistically significant, and a value of $0.1 < p < 0.05$ was considered marginally significant.

# 3. RESULTS*

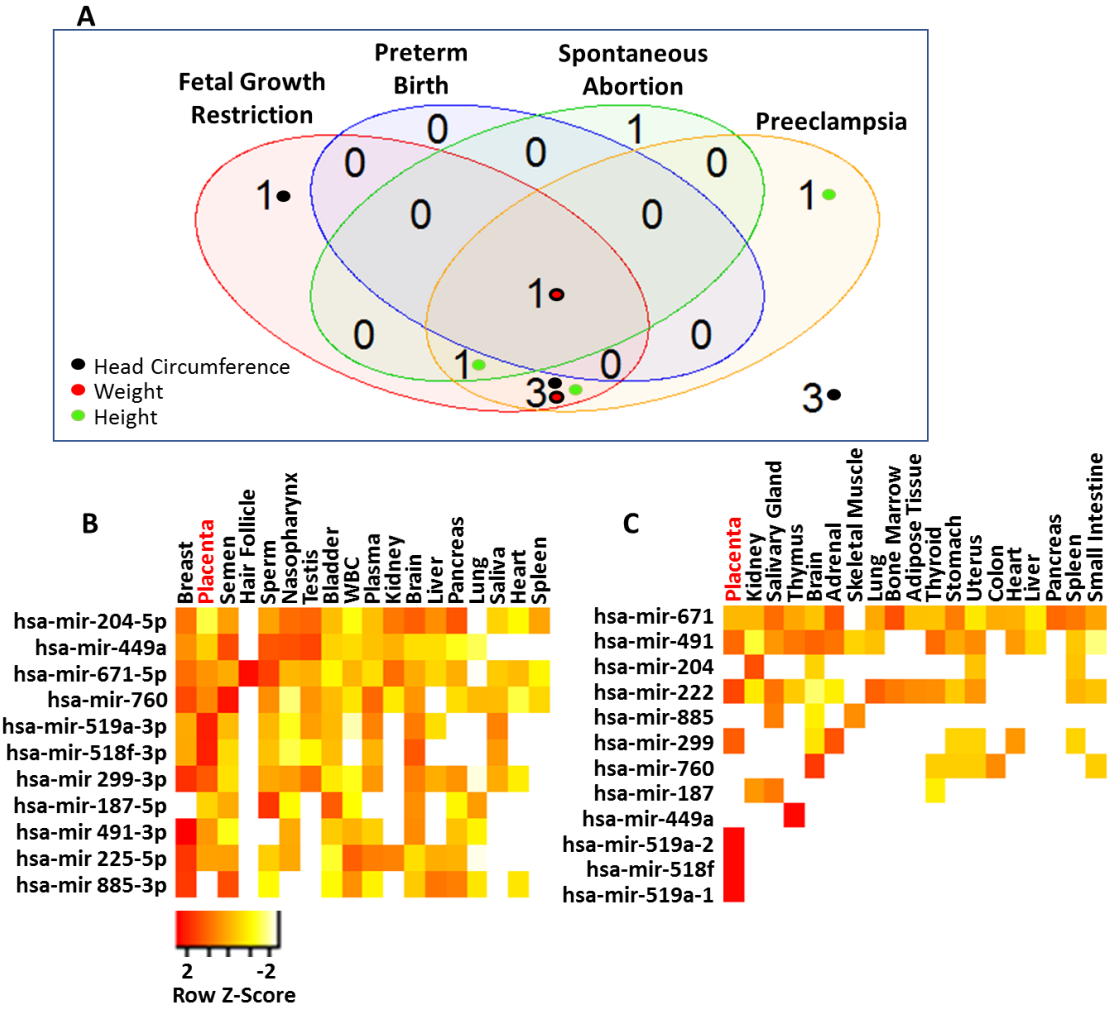


**Figure 3: HEamiRNAs are placentally enriched and associated with gestational pathologies**
A) Venn diagram on number of HEamiRNAs reported to be associated with different gestational pathologies. Inset colored circles represent the corresponding sex and gestational age-adjusted growth parameters these miRNAs were correlated with. Of the 22 studies queried, 11 (50%) utilized unbiased screenings for miRNA expression.
B) Heatmap of mature HEamiRNA expression and C) pri-HEamiRNA expression across different tissues resulting from secondary analysis of publicly available RNA-sequencing data. Legend depicts row-centered Z-score

* Part of this chapter is reprinted with permission from "Maternal circulating miRNAs that predict infant FASD outcomes influence placental maturation" by Tseng et al., 2019. *Life Science Alliance*, Vol. 2, © 2019 by Tseng et al.

### 3.1 HEamiRNAs are implicated in placental-associated pathologies

Outside of our report that elevated HEamiRNA levels predict infant outcomes following PAE, few other studies have investigated expression of these miRNAs in the context of PAE or other potentially toxic prenatal exposures (29-36). Given our prediction that HEamiRNAs interfere with signaling pathways governing fetal and placental development (11), we conducted a literature review of reports on HEamiRNA levels in gestational pathologies which, as with PAE, include aberrant placentation as an etiological factor (37-39). Surprisingly, placental and plasma levels of 8 out of 11 of these HEamiRNAs were significantly dysregulated in one or more of these gestational pathologies with expression of the majority of these 8 miRNAs altered in both fetal growth restriction and preeclampsia (Figure 3A) (33, 34, 36, 40-57), both of which are characterized by poor placental invasion as an etiological factor (58-64).

### 3.2 HEamiRNAs explain variance in infant growth outcomes due to PAE

Given the association of individual HEamiRNAs with gestational pathologies, we sought to determine if circulating HEamiRNAs levels could explain the variance in sex and gestational age-adjusted neonatal height, weight and head circumference in our Ukrainian birth cohort, which are growth measures sensitive to in utero environment (65). We found that 8 of the HEamiRNAs, each significantly explained between 7 to 19% of infant variation in these growth measures (Table 2). Furthermore, 7 of these miRNAs were also associated with fetal growth restriction and preeclampsia as identified by our literature review. Additionally, only 1 of the 3 miRNAs not previously-reported to be associated with gestational pathologies was correlated with measures of fetal growth and

development in our dataset (Figure 3A). Interestingly, a multivariate statistical regression model that accounted for levels of all 11 HEamiRNAs together, explained a far greater proportion of infant variance, between 24-31%, in all three growth measures than accounting for them individually (Table 3).

### 3.3 HEamiRNAs are transcribed preferentially in the placenta

Data extracted from publicly available gene expression profiling datasets (66) show that HEamiRNAs as well as their unprocessed precursor transcripts, HEapri-miRNAs, are enriched in placenta compared to other tissues, suggesting that the placenta itself transcribes these miRNAs and may be a significant contributory tissue to maternal circulating HEamiRNAs (Figures 3B and C). Since chorionic villi are immersed in maternal blood, it is possible that the placenta is both a source and a target of maternal HEamiRNAs. Moreover, since HEamiRNAs are also associated with gestational pathologies caused by poor placental invasion, these HEamiRNAs may also constitute an intra-placental paracrine signal to coordinate the (mal)adaptive response of tissues to PAE. We therefore assessed in rodent and primate models, whether PAE could result in impaired EMT, and if HEamiRNAs could explain the effects of PAE on placental EMT-associated gene expression.

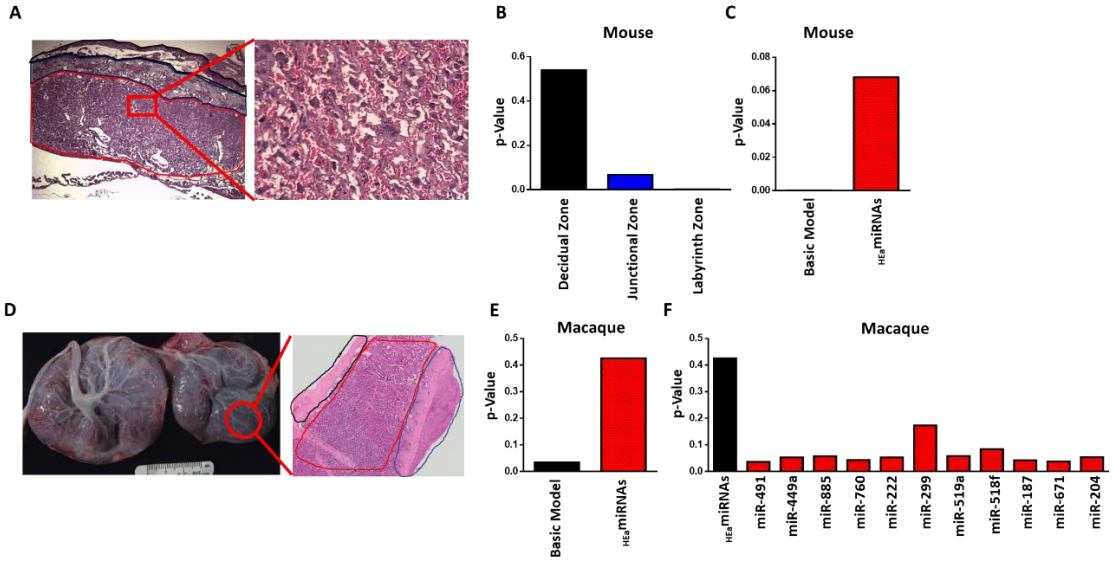


**Figure 4: $_{HEa}$miRNAs mediate the effect of PAE on EMT pathway members in mouse and macaque placentas.**

A) Histological image of GD14 mouse placenta. Outlined in red is the labyrinth zone, blue is the junctional zone, black is the decidual zone. Inset is a high magnification image of the labyrinth zone.

B) MANOVA of gene expression of core EMT pathway members in different regions of the mouse placenta in control and PAE mice (n=29 samples).

C) MANCOVA of gene expression of core EMT pathway members in the mouse placental labyrinth zone before (Basic Model) and after accounting for the expression of $_{HEa}$miRNAs (n=29 samples).

D) Gross anatomy photograph of the primary (left) and secondary (right) lobes of a GD135 macaque placenta. Outlined in red is an individual cotyledon from the secondary lobe. Inset is a full thickness hematoxylin and eosin stained histological section of a representative cotyledon with the fetal membranes outlined in black, villous tissue outlined in red and maternal decidua in blue.

E) MANCOVA of gene expression of core EMT pathway members in placental cotyledons of PAE and control macaques, accounting for the expression of $_{HEa}$miRNAs collectively (n=23 samples).

F) MANCOVA of gene expression of core EMT pathway members in macaque placentas after accounting for expression of $_{HEa}$miRNAs individually (n=23 samples).

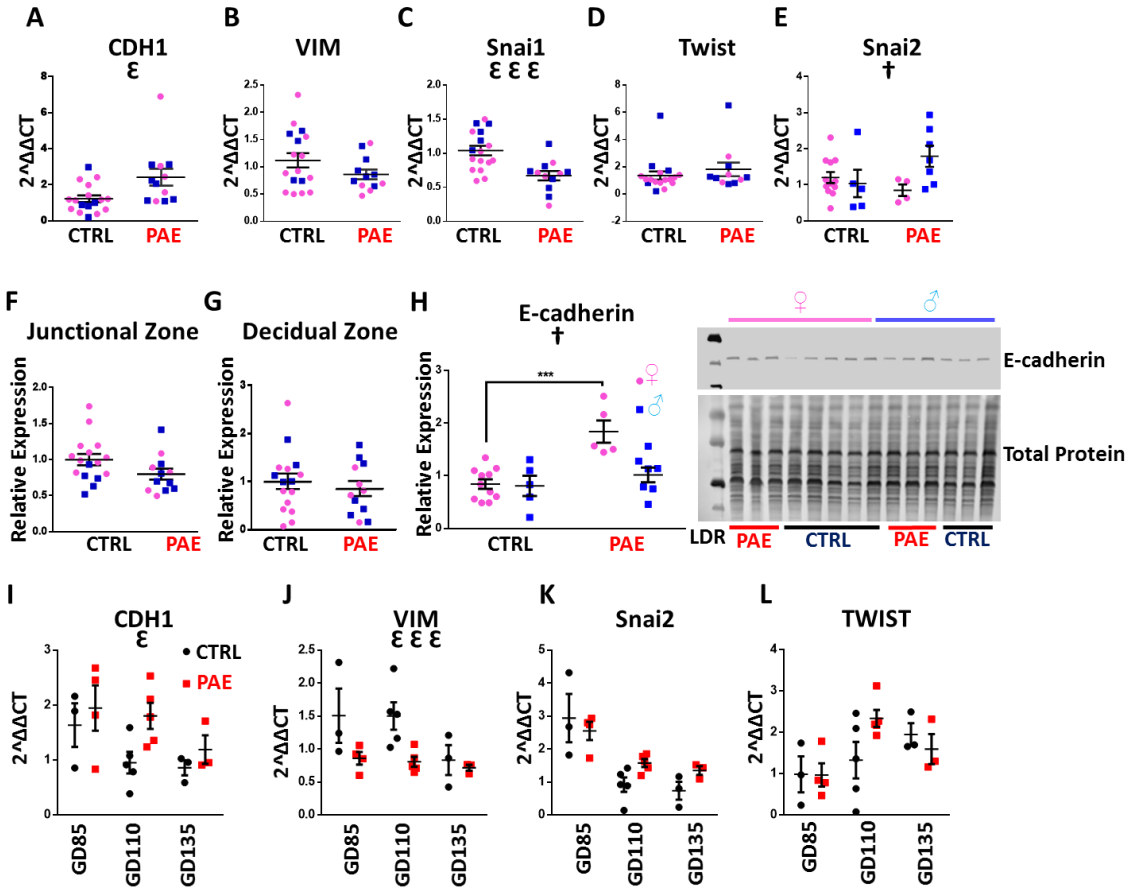


**Figure 5: PAE interferes with the EMT pathway in mouse and macaque placentas**
Expression of **A)** *CDH1*, **B)** *VIM*, **C)** *SNAI1*, **D)** *TWIST*, and **E)** *SNAI2* in the placental labyrinth zone of PAE and control mice (n=5-12 samples per group).
Densitometric quantification of E-cadherin expression in the in **F)** junctional, **G)** decidual, and **H)** labyrinth zone of PAE and control mice as well as representative blot of E-cadherin expression and total protein expression (right, n=5-12 samples per group).
Expression of **I)** *CDH1*, **J)** *VIM*, **K)** *SNAI2*, and **L)** *TWIST* transcripts in PAE and Control macaque placental cotyledons (n=3-5 samples per group).
Results are expressed as the mean ± SEM, LDR=Molecular Weight Ladder; ANOVA: significant main effect of PAE [$^{\varepsilon}p<0.05$, $^{\varepsilon\varepsilon\varepsilon}p<0.001$], significant interaction effect (sex by PAE, [$^{\dagger}p<0.05$]). For post-hoc analysis, ***$p<0.001$ by Tukey's HSD.

### 3.4 $_{HEa}$miRNAs moderate PAE's effects on EMT pathway members

EMT, in trophoblasts, is characterized by the disappearance of epithelial markers like E-cadherin and the appearance of the mesenchymal markers like the intermediate filament, vimentin, a process that is controlled by the expression of key mesenchymal

determination transcription factors, Snail1 and 2 and TWIST, as extensively described (13, 17, 18, 67-70). These five markers have been used extensively to assess EMT in a variety of model systems and therefore our studies utilized these markers to investigate the effects of alcohol and $_{HEa}$miRNAs on trophoblast EMT.

In the first analysis, using a murine model of PAE that mimicked moderate to binge-type alcohol consumption throughout early and mid-pregnancy, we fractionated GD14 placenta into three zones: the cytotrophoblast and syncytiotrophoblast rich labyrinth zone, the glycogen and spongiotrophoblast rich junctional zone, and the decidual zone comprising the endometrial contribution to the placenta (Figure 4A). Multivariate analysis of variance (MANOVA) for expression of these five core genes in the EMT pathway within placental trophoblasts, revealed a significant effect of ethanol exposure on EMT pathway member expression selectively within the labyrinth zone (Pillai's trace statistic, $F_{(5,21)}=6.85$, $p<0.001$, Figure 4B) but not within the junctional or decidual zones. Post-hoc univariate ANOVA indicated ethanol exposure specifically elevated *CDH1* ($F_{(1,25)}=7.452$, $p=0.011$), which encodes epithelial E-cadherin, whereas expression of the pro-mesenchymal transcription factor *SNAI1* was significantly reduced ($F_{(1,25)}=21.022$, $p=0.0001$). We also observed a significant interaction between fetal sex and PAE on expression of *SNAI2* ($F_{(1,25)}=2.18$, $p=0.047$) and a trend towards decreased expression of the terminal mesenchymal marker *VIM* (Vimentin, $F_{(1,25)}=2.749$, $p=0.11$), while there was no effect on *TWIST* expression (Figures 5A-E). Consistent with our gene expression data, E-cadherin protein levels were significantly elevated in the labyrinth zone of PAE placenta ($F_{(1,24)}=31.63$, $p=0.0005$), while not in the junctional or decidual

zones (Figure 5F-H). However, when we controlled for expression of the 8 mouse homologues of $_{HEa}$miRNAs as a covariate, using multivariate analysis of covariance (MANCOVA), ethanol's effect on EMT became marginally nonsignificant (Pillai's trace, $F_{(5,21)}$=2.713, p=0.068) (Figure 4C), suggesting that these miRNAs only partially mediate effects of PAE on EMT pathway members in mice.

To determine if effects of PAE on EMT pathway members in placenta are broadly conserved throughout mammalian evolution, we adopted a non-human primate (macaque) model of moderate to binge-type alcohol consumption. Placental tissues were isolated from GD85, GD110, and GD 135 placenta (Figure 4D), which spans the human equivalent of mid-second to mid-third trimester (Figure 1C). There was a significant effect of ethanol exposure on expression of core EMT mRNA transcripts by MANOVA (Pillai's trace statistic, $F_{(4,9)}$=4.229 p=0.045, Figure 4E). Consistent with our findings in mouse, post-hoc univariate ANOVA indicated that in primate placenta, ethanol exposure significantly increased *CDH1* expression ($F_{(1,12)}$=4.866, p=0.048) whereas *VIM* expression was significantly reduced ($F_{(1,12)}$=12.782, p=0.0004), suggesting that, as in the mouse, PAE also impairs EMT in the primate placenta. Interestingly, there was no effect on *SNAI2* or *TWIST* expression (Figures 5I-L). As in mice, accounting for expression of $_{HEa}$miRNAs together as a covariate abolished the significant effect of PAE on EMT, though to a greater degree than mice (Pillai's trace, $F_{(1,1)}$=1.605, p=0.425, Figure 4E). Interestingly, accounting for expression of individual $_{HEa}$miRNAs did not explain the effects of PAE on placental EMT, suggesting that $_{HEa}$miRNAs act in concert to mediate the effect of PAE on EMT in primate placenta (Figure 4F). PAE limited to the

peri-conceptional period in rats also influenced expression of EMT core transcripts (Figure 1B and Figures 6A-E).

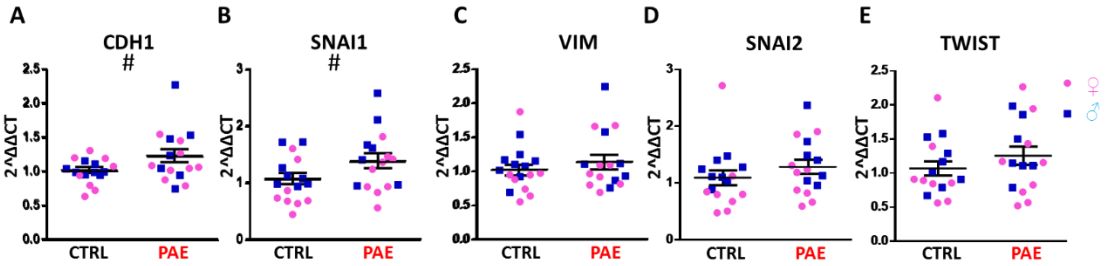


**Figure 6: PAE and expression of core EMT transcripts in rat placenta**
**A)** Expression of CDH1, **B)** Snai1, **C)** VIM, **D)** Snai2, and **E)** TWIST in the placental labyrinth zone of PAE and control rats.
Results are expressed as expressed as the mean ± SEM, n=8 samples per group; ANOVA: significant main effect of PAE [#p<0.05].

Collectively, our data suggests PAE induced impairment of EMT in the trophoblastic compartment of placentae is conserved between rodents and non-human primates and that $_{HEa}$miRNAs, particularly in primates, may moderate the effect of PAE on placental EMT. Consequently, subsequent studies focused on the collective role of $_{HEa}$miRNAs, either on basal or on alcohol-influenced placental trophoblast growth, invasion, and the maturation of physiological function.

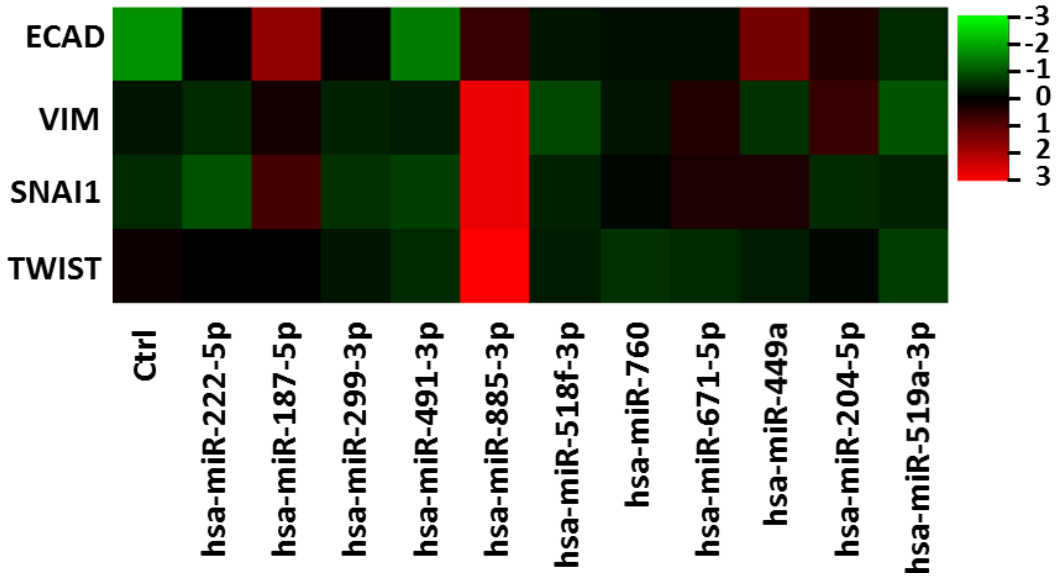


**Figure 7: Individual $_{HEa}$miRNAs do not affect EMT pathway in BeWO cytotrophoblasts**
Heatmap for expression of core members of the EMT pathway following overexpression of individual $_{HEa}$miRNAs or a control (Ctrl) miRNA. Scale for heatmap coloration, right, depicts row-centered Z-score, n=10 samples per group.

### 3.5 $_{HEa}$miRNAs impair EMT pathway member expression in a model of human cytotrophoblasts

To investigate whether $_{HEa}$miRNAs collectively interfere with the EMT pathway, as suggested by our *in vivo* data, we measured expression of core members of the EMT pathway after transfecting $_{HEa}$miRNA mimics and antagomirs into BeWO cytotrophoblasts. Cytotrophoblasts normally undergo EMT to become invasive trophoblasts, which we also modelled using the HTR8 human extravillous trophoblast cell line. We initially overexpressed each of the 11 $_{HEa}$miRNAs individually, to determine whether any of them could alter mRNA transcripts for EMT pathway members. However, we did not observe any significant effects due to overexpression of individual miRNAs (Figure 7), consistent with our findings in the primate PAE model that individual miRNAs did not explain the effects of ethanol on EMT. In contrast,

transfection of pooled $_{HEa}$miRNAs into cytotrophoblasts (Figure 8A) significantly increased *CDH1* expression ($F_{(1,36)}$=30.08, p<0.0001). Interestingly, expression of the pro-mesenchymal transcription factors *TWIST* and *SNAI1* were also significantly reduced, but only in the context of concomitant 320 mg/dL ethanol treatment, pointing to an interaction effect between $_{HEa}$miRNAs and ethanol ($F_{(1,36)}$= 5.650 and 5.146 respectively, p=0.023 and p=0.029, Figures 8B-E). Consistent with our qPCR data, transfection of $_{HEa}$miRNAs also significantly increased E-cadherin protein expression ($F_{(1,20)}$=33.86, p<0.0001, Figure 8F). We were unable to detect *SNAI2* transcript expression or vimentin protein expression in these cells, consistent with previous reports (71).

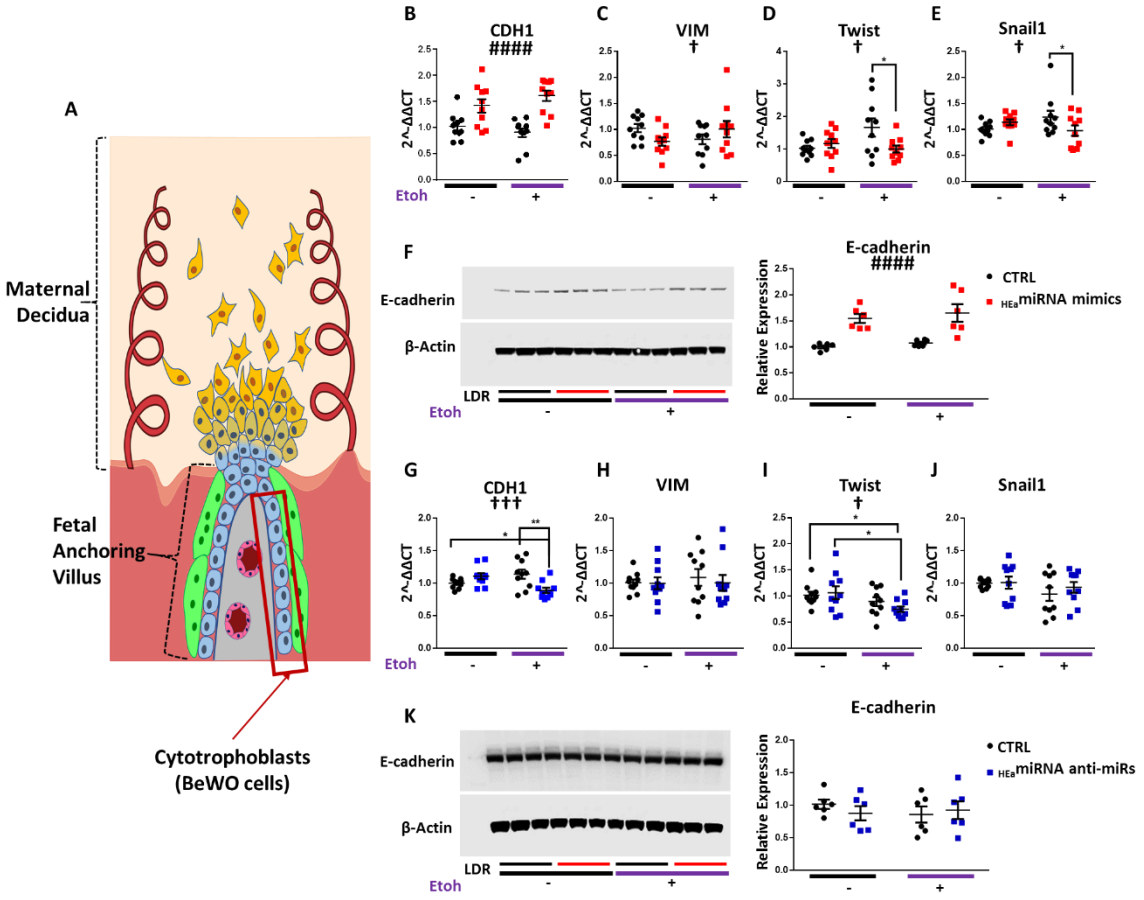


**Figure 8: $_{HEa}$miRNAs interfere with the EMT pathway in BeWO cytotrophoblasts**

**A)** Diagram of a placental anchoring villous and maternal decidua with the boxed area denoting cytotrophoblasts.

Expression of **B)** *CDH1*, **C)** *VIM*, **D)** *TWIST*, and **E)** *SNAI1* transcripts **F)** and densitometric quantification of E-cadherin protein levels in BeWO cytotrophoblasts following $_{HEa}$miRNAs or control miRNA overexpression with or without concomitant 320 mg/dL ethanol exposure.

**G)** Expression of *CDH1*, **H)** *VIM*, **I)** *TWIST*, and **J)** *SNAI1* transcripts **K)** and densitometric quantification of E-cadherin protein levels in BeWO cytotrophoblasts following $_{HEa}$miRNAs or control hairpin inhibitor transfection with or without concomitant 320 mg/dL ethanol exposure. Results are expressed as the mean ± SEM, LDR=Molecular Weight Ladder, n=10 samples per group; ANOVA: significant main effect of $_{HEa}$miRNA transfection [$^{####}$p<0.0001], significant interaction effect ($_{HEa}$miRNA by 320mg/dL ethanol, [$^{†}$p<0.05, $^{†††}$p<0.001]). For post-hoc analysis *p<0.05, **p<0.01 by Tukey's HSD.

Whereas transfection of $_{HEa}$miRNA mimics increased *CDH1* expression, transfection of pooled antagomirs to $_{HEa}$miRNAs, significantly reduced CDH1 expression, only in the context of 320 mg/dL ethanol co-exposure (post-hoc Tukey's HSD, p=0.005), consistent with an overall statistically significant interaction effect

between ethanol exposure and HEamiRNA inhibition ($F_{(1,36)}$=13.51, p=0.0008, Figure 8G). However, expression of *TWIST* was also decreased in this context and there was no significant difference in E-cadherin protein expression relative to the control (Figure 8H-K). Thus, our data suggest that, increasing HEamiRNA levels impairs EMT pathway members in cytotrophoblasts whereas inhibiting their action has a more restricted effect on EMT pathway members.

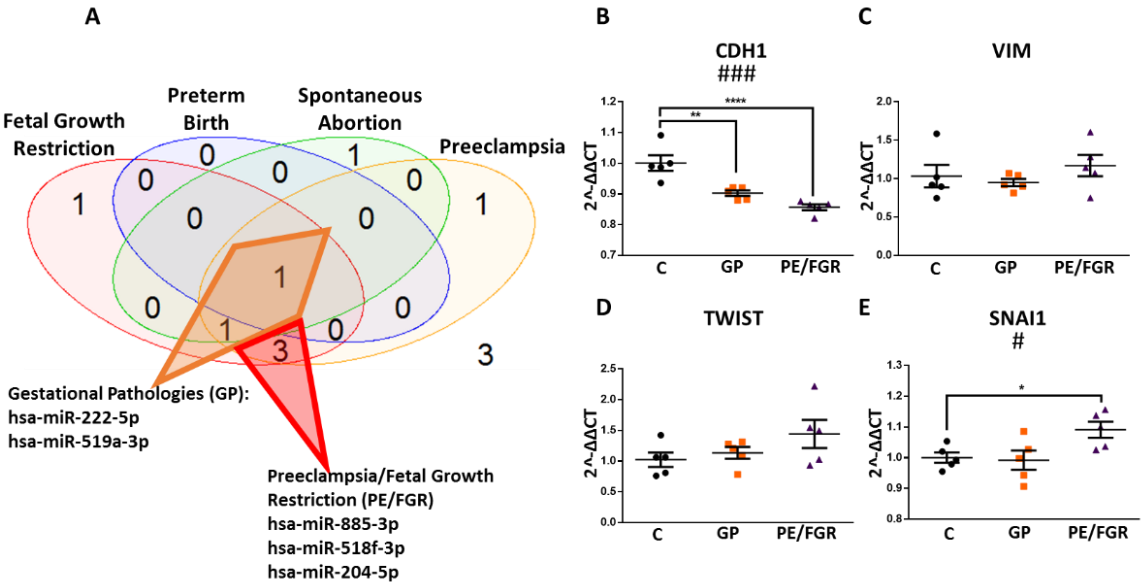


**Figure 9: HEamiRNAs subpools have different effect on the EMT pathway in BeWO cytotrophoblasts**
**A)** Venn diagram with the diamond indicating HEamiRNAs broadly implicated in gestational pathologies and the triangle outlining miRNAs implicated in preeclampsia and fetal growth restriction. Expression of **B)** *CDH1* **C)** *VIM* **D)** *TWIST* and **E)** *SNAI1* transcripts following control (**C**), [hsa-miR-222-5p and hsa-miR-519a-3p] (GP), or [hsa-miR-885-3p, hsa-miR-518f-3p, and hsa-miR-204-5p] (PE/FGR) overexpression. Results are expressed as expressed as the mean ± SEM, n=5 samples per group; ANOVA: significant treatment effect [$^{\#}p<0.05$, $^{\#\#\#}p<0.001$]. For post-hoc analysis, *p<0.05, **p<0.01, and ****p<0.0001 by Dunnett's Multiple Comparisons.

We next sought to determine if more restricted subsets of HEamiRNAs could recapitulate the effects of HEamiRNAs collectively on EMT. Thus, we overexpressed hsa-miR-222-5p and hsa-miR-519a-3p, which are implicated in preeclampsia and fetal

growth restriction, as well as hsa-miR-885-3p, hsa-miR-518f-3p, hsa-miR-204-5p, which are implicated in preeclampsia, fetal growth restriction, and spontaneous abortion or preterm labor (Figure 9A). In contrast to the collective action for all $_{HEa}$miRNAs, exposure to each of these pools resulted in significant decreases in CDH1 expression ($F_{(2,12)=}$20.12, p=0.0001). The pool including hsa-miR-885-3p, hsa-miR-518f-3p, hsa-miR-204-5p also significantly increased Snai1 ($F_{(2,12)}$=4.604, p=0.0328; Dunnett's post-hoc p=0.0497, Figure 9B-E). These data suggest that $_{HEa}$miRNAs include sub-groups of miRNAs that have the potential to partly mitigate the effects of elevating the entire pool. However, the potential protective effects of these sub-groups are masked by the collective function of the entire group of $_{HEa}$miRNAs.

### 3.6 $_{HEa}$miRNAs impair EMT member expression in a model of human extravillous trophoblasts

We next investigated the effect of $_{HEa}$miRNAs on EMT in HTR-8/SVneo extravillous trophoblast-type cells (Figure 10A). Transfecting pooled $_{HEa}$miRNA mimics into extravillous trophoblasts significantly decreased *VIM* expression ($F_{(1,36)}$=28.43, p<0.0001). Expression of pro-mesenchymal transcription factors *SNAI2* was also reduced ($F_{(1,36)}$= 64.88 respectively, p<0.0001). As with cytotrophoblasts, expression of SNAI1 and *TWIST* were reduced only with 320 mg/dL ethanol co-exposure (post-hoc Tukey's HSD, p =0.027 and p<0.0001 respectively) indicating an interaction effect ($F_{(1,36)}$=4.21 and 5.18, p=0.048 and 0.029 respectively, Figures 10B-E). Consistent with our qPCR data, Vimentin protein expression was also significantly reduced ($F_{(1,20)}$=9.535, p=0.006, Figure 10F). Interestingly, there was also a main effect of

alcohol exposure on decreasing vimentin protein expression ($F_{(1,20)}$=7.303, p=0.014). We were unable to detect expression of *CDH1* transcript, or its E-cadherin protein product, in extravillous trophoblasts, consistent with previous reports (71).

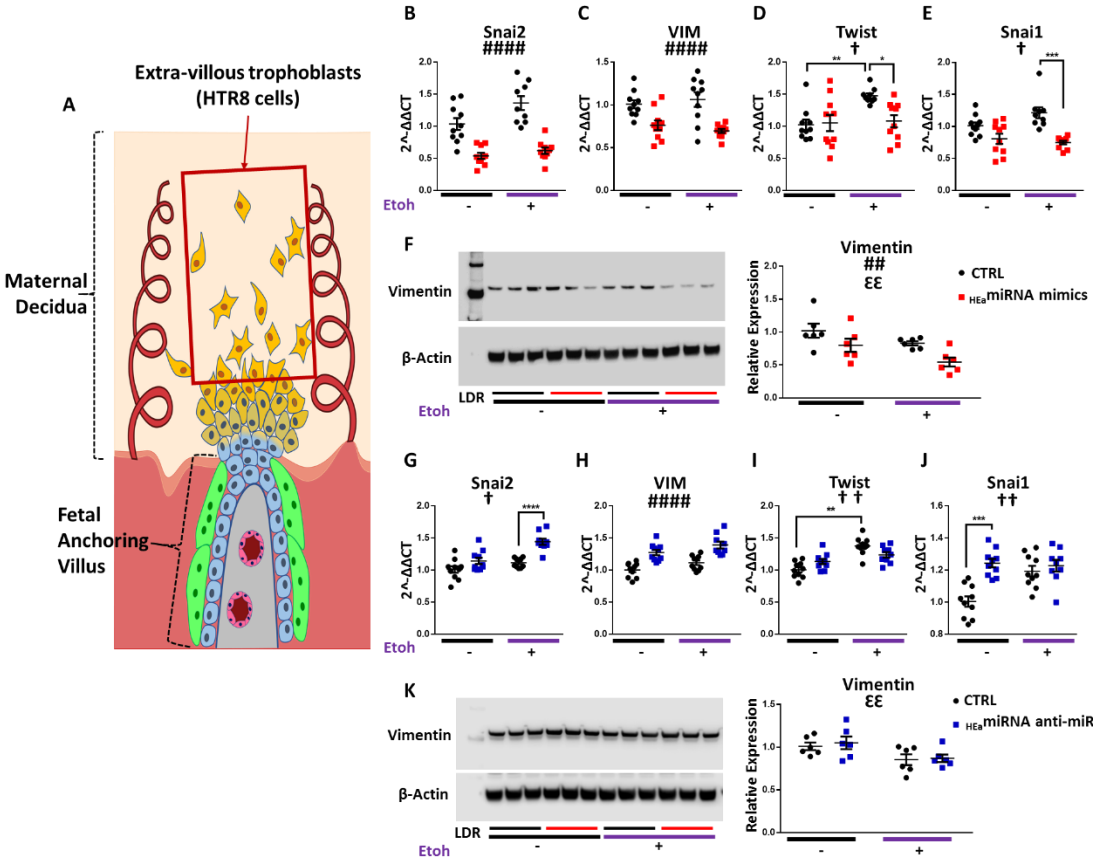


**Figure 10: $_{HEa}$miRNAs interfere with the EMT pathway in HTR8 extravillous trophoblasts**

**A)** Diagram of a placental anchoring villous and maternal decidua with the boxed area denoting extravillous trophoblasts.
Expression of **B)** *SNAI2* **C)** *VIM* **D)** *TWIST* and **E)** *SNAI1* transcripts **F)** as well as densitometric quantification of Vimentin protein levels in HTR8 extravillous trophoblasts following $_{HEa}$miRNAs or control miRNA overexpression with or without concomitant 320 mg/dL ethanol exposure.
Expression of **G)** *SNAI2* **H)** *VIM* **I)** *TWIST* and **J)** *SNAI1* transcripts **K)** as well as densitometric quantification of Vimentin protein levels in HTR8 extravillous trophoblasts following $_{HEa}$miRNA or control hairpin inhibitor transfection with or without concomitant 320 mg/dL ethanol exposure.
Results are expressed as the mean ± SEM, LDR=Molecular Weight Ladder, n=10 samples per group; ANOVA: significant main effect of $_{HEa}$miRNA transfection [$^{\#\#}$p<0.01, $^{\#\#\#\#}$p<0.0001], significant main effect of 320mg/dL ethanol exposure [$^{ƐƐ}$p<0.01], significant interaction effect ($_{HEa}$miRNA by 320mg/dL ethanol, [$^{\dagger}$p<0.05, $^{\dagger\dagger}$p<0.01]). For post-hoc analysis *p<0.05, **p<0.01, ***p<0.001, and ***p<0.0001 by Tukey's HSD.

In contrast to $_{HEa}$miRNA mimics, transfecting pooled antagomirs significantly increased *VIM* expression ($F_{(1,35)}$=42.56, p<0.0001). Likewise, there were interaction effects for *SNAI1* and *SNAI2* ($F_{(1,35)}$=10.31 and 4.86, p=0.01 and p=0.034 respectively), whereby antagomir transfection increased expression of Snai2 in the context of 320mg/dL ethanol co-exposure (post-hoc Tukey's HSD, p<0.0001) and Snai1 under basal conditions (post-hoc Tukey's HSD, p<0.0001)(Figures 10G-J). Despite our qPCR data, we did not observe significant differences in vimentin protein expression between treatment groups (Figure 10K). Collectively, our data indicate that increased trophoblastic $_{HEa}$miRNA levels favors an epithelial phenotype, whereas inhibiting their action promotes a mesenchymal phenotype.

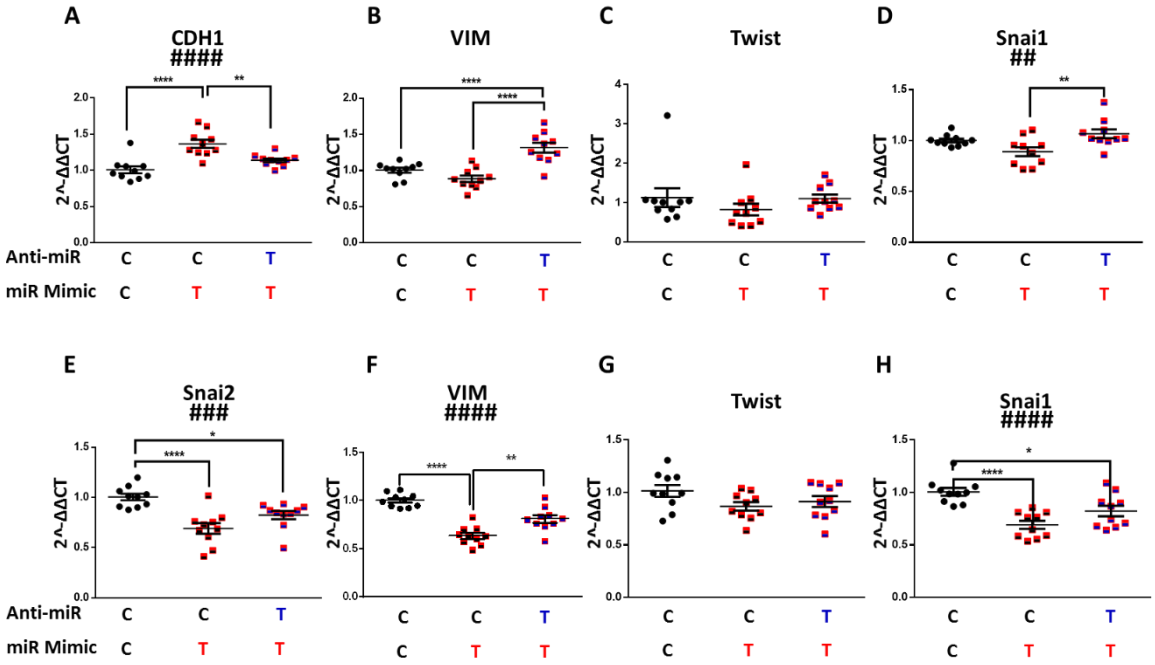


**Figure 11: Antagomirs prevent $_{HEa}$miRNA induced impairment of EMT**

Expression of **A)** *CDH1* **B)** *VIM* **C)** *TWIST* and **D)** *SNAI1* transcripts following control or $_{HEa}$miRNA hairpin inhibitor transfection followed by control or $_{HEa}$miRNA overexpression in BeWO cytotrophoblasts. Expression of **E)** *CDH1* **F)** *VIM* **G)** *TWIST* and **H)** *SNAI1* transcripts following control or $_{HEa}$miRNA antagomir transfection followed by control or $_{HEa}$miRNA overexpression in HTR8 extravillous trophoblasts.

In subheadings: **C** denotes control miRNA mimic or hairpin whereas **T** denotes $_{HEa}$miRNA mimic or hairpin inhibitor. Results are expressed as expressed as the mean ± SEM, n=10 samples per group; ANOVA: significant treatment effect [$^{\#\#}p<0.01$, $^{\#\#\#}p<0.001$, $^{\#\#\#\#}p<0.0001$]. For post-hoc analysis, $*p<0.05$, $**p<0.01$, $***p<0.001$, $****p<0.0001$ by Tukey's HSD.

### 3.7 Antagomirs prevent $_{HEa}$miRNAs' inhibition of EMT pathway members

We next investigated if pretreating trophoblasts with pooled $_{HEa}$miRNA antagomirs could prevent inhibition of the EMT pathway caused by transfecting $_{HEa}$miRNA mimics. *CDH1* expression in cytotrophoblasts transfected with control antagomir, and subsequently transfected with control mimic, was not significantly different from those transfected with $_{HEa}$miRNA antagomirs and $_{HEa}$miRNA mimics. However, *CDH1* was significantly elevated in cytotrophoblasts transfected with control

antagomir and $_{HEa}$miRNA mimics (post-hoc Tukey's HSD, n=10 samples per group, p=0.004). Likewise, cells pre-transfected with $_{HEa}$miRNA antagomirs had significantly higher *SNAI1* and *VIM* expression than those pre-transfected with control antagomir and subsequently transfected with $_{HEa}$miRNA mimics (post-hoc Tukey's HSD, n=10 samples per group, p=0.007 and p<0.0001 respectively) (Figure 11A-D).

Furthermore, *VIM* expression in extravillous trophoblasts pre-transfected with control antagomir, and subsequently transfected with control mimic, was not significantly different from those transfected with $_{HEa}$miRNA antagomirs and $_{HEa}$miRNA mimics. However, *VIM*, *SNAI1*, and *SNAI2* expression were significantly reduced in cytotrophoblasts transfected with control antagomir and $_{HEa}$miRNA mimics (post-hoc Tukey's HSD, n=10 samples per group, p<0.0001, Figure 11E-H). Thus, our data suggest that pretreating cells with $_{HEa}$miRNA antagomirs prevents inhibition of EMT pathway members resulting from transfection with $_{HEa}$miRNA mimics in cytotrophoblasts and extravillous trophoblasts.

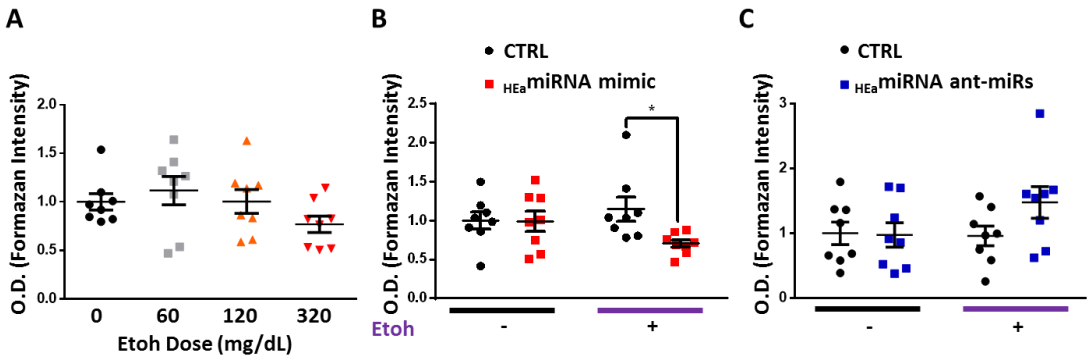


**Figure 12: $_{HEa}$miRNA impair extravillous trophoblast invasion**

Transwell invasion of HTR8 extravillous trophoblasts following **A)** 0, 60, 120, and 320mg/dL ethanol exposure or transfection with **B)** $_{HEa}$miRNA mimics or **C)** hairpin inhibitors with or without concomitant 320 mg/dL ethanol exposure.

O.D. = optical density, results are expressed as expressed as the mean ± SEM; n=10 samples per group; *p<0.05 by Unpaired T-test

### 3.8 $_{HEa}$miRNAs impair extravillous trophoblast invasion

Functionally, inhibition of the EMT pathway should reduce trophoblast invasiveness. Thus, we performed a transwell invasion assay using HTR8 extravillous trophoblasts transfected with $_{HEa}$miRNA mimics and antagomirs. While ethanol exposure by itself did not impair trophoblast invasion (Figure 12A), there was a marginally significant interaction effect between ethanol exposure and $_{HEa}$miRNA mimic transfection ($F_{1,28}=3.418$, $p=0.075$). Thus, a planned comparison indicated that transfection with $_{HEa}$miRNA mimics significantly reduced trophoblast invasion in the context of 320 mg/dL ethanol co-exposure, relative to the control mimics ($t(14)=2.762$, $p=0.015$), consistent with our data demonstrating $_{HEa}$miRNAs interfere with the EMT pathway (Figure 12B). Contrastingly, transfecting $_{HEa}$miRNA antagomirs increased invasion in the context of 320 mg/dL ethanol co-exposure, though this effect was only marginally significant ($t(14)=1.805$, $p=0.093$, Figure 12C).

### 3.9 $_{HEa}$miRNAs retard trophoblast cell cycle progression

Given the proliferative nature of cytotrophoblasts, and the intimate relationship between EMT and cell cycle (72, 73), we assessed the effects of ethanol and $_{HEa}$miRNAs on BeWO cytotrophoblast cell cycle. After pulse-labeling cells with the nucleic acid analog, 5-Ethynyl-2'-deoxyuridine (EdU), for 1-hour, we found that individually transfecting 6 of the $_{HEa}$miRNA mimics increased EdU incorporation (Unpaired t-test, $p<0.05$, FDR correction), suggesting an overall increased rate of DNA synthesis (Figure 13). Consistent with the increased rates of DNA synthesis resulting from individual $_{HEa}$miRNA mimic transfection, individual transfection of $_{HEa}$miRNAs antagomirs generally reduced EdU incorporation, though only the antagomir to hsa-miR-760 did so significantly ($t(110)=3.059$, $p=0.003$, FDR correction) (Figure 13).

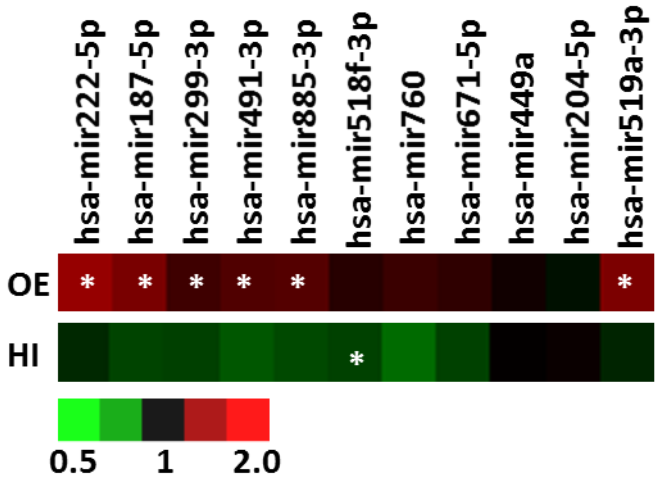


**Figure 13: Individual $_{HEa}$miRNAs interfere with trophoblast cell cycle dynamics**
Heatmap for degree of EdU incorporation in BeWO cytotrophoblasts following individual $_{HEa}$miRNA overexpression (top, OE) or transfection with individual $_{HEa}$miRNA hairpin inhibitors (bottom, HI). Scale for heatmap coloration, right, denotes fold change of EdU incorporation intensity relative to control mimic or hairpin transfection. N=6 samples per group, white asterisks denote $_{HEa}$miRNA mimics or hairpin inhibitors that had a significant effect, $p<0.05$, Student's T-test, on degree of EdU incorporation.

Contrastingly, simultaneous transfection of $_{HEa}$miRNAs significantly reduced EdU incorporation ($F_{(1,26)}=59.69$, $p<0.0001$, Figure 14A). Interestingly, simultaneous administration of antagomirs also reduced EdU incorporation, as observed with the pooled $_{HEa}$miRNAs mimics ($F_{(1,26)}=34.83$, $p=0.0005$, Figure 14B). This reduction in EdU synthesis mirrors the effects of increasing concentrations of ethanol ($R^2=0.304$, $p=0.012$) (Figures 14C).

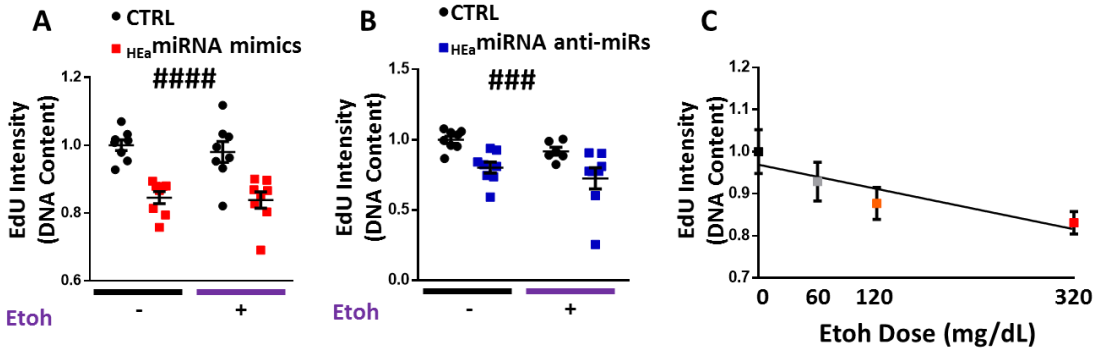


**Figure 14: $_{HEa}$miRNAs inhibit the rate of DNA synthesis in trophoblasts**

**A)** Degree of EdU incorporation following control and $_{HEa}$miRNA overexpression.

**B)** Degree of EdU incorporation following control and $_{HEa}$miRNA hairpin inhibitor transfection.

**C)** Degree of EdU incorporation in BeWO cytotrophoblasts following 0, 60, 120, and 320mg/dL ethanol exposure. n=5 samples per group.

ANOVA: significant main effect of $_{HEa}$miRNA transfection [$^{###}p<0.001$, and $^{####}p<0.0001$].

To further characterize the coordinated effect of $_{HEa}$miRNAs on cytotrophoblast cell cycle, we pulse-labeled cells with EdU for 1-hour and, post-fixation, labelled them with 7-Aminoactinomycin D (7AAD) to segregate cells into three groups: $G_0/G_1$ (7AADlow, EDU-), S (EDU+), and $G_2$/M (7AADhigh, EDU-). Both 120 mg/dL and 320 mg/dL ethanol exposures significantly decreased the proportion of cells in S-phase, while 320 mg/dL exposure increased the proportion of cells in $G_2$/M-phase, consistent with the observed reduction in the rate of DNA synthesis (Figure 15A). Similar, to the effects of ethanol exposure, pooled $_{HEa}$miRNA mimic administration also significantly decreased the proportion of cells in S-phase ($F_{(1,28)}=52.78$, $p<0.0001$) while increasing the proportion of cells the $G_2$/M-phase ($F_{(1,28)}=8.395$, $p=0.007$) and exacerbated alcohol's effects on the cell cycle (Figure 15B). Interestingly, pooled $_{HEa}$miRNA antagomir administration also reduced the proportion of cells in S-phase ($F_{(1,26)}=14.98$,

p=0.0007) and increased the proportion of those in $G_2$/M-phase ($F_{(1,26)}$=12.38, p=0.002) (Figure 15C).

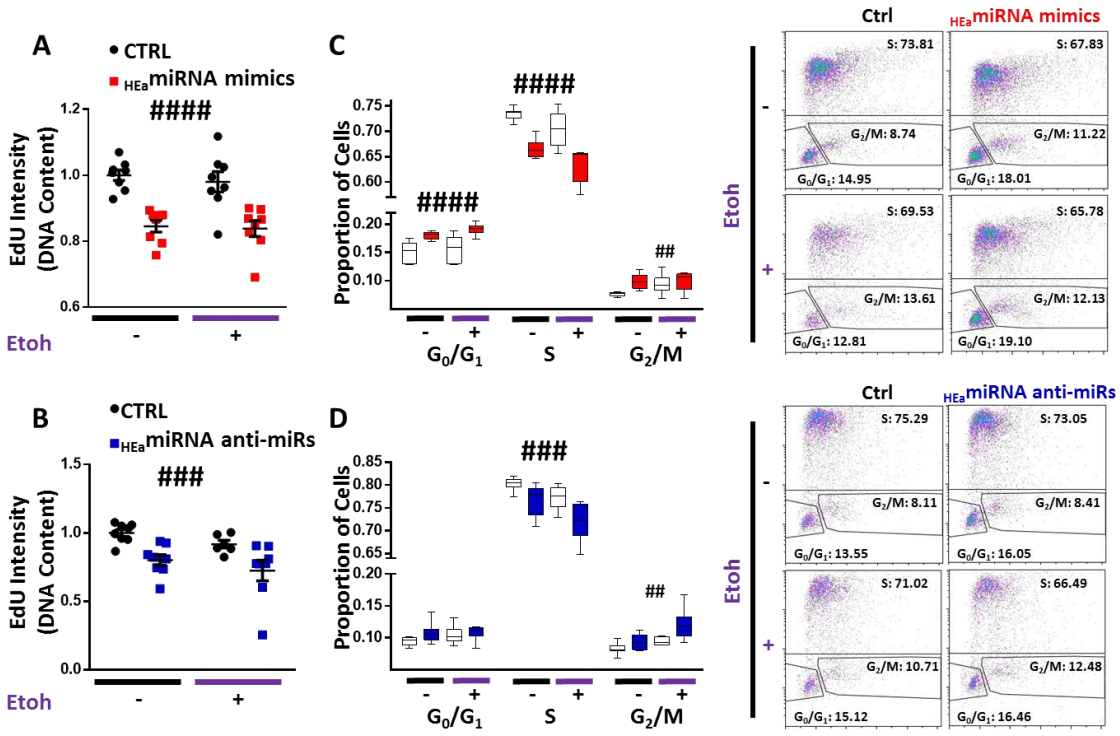


**Figure 15: $_{HEa}$miRNA cause cell cycle retardation in trophoblasts**

**A)** Proportion of BeWO cytotrophoblasts in $G_0/G_1$, S, or $G_2$/M phase of the cell cycle following 0, 60, 120, and 320mg/dL ethanol exposure.

**B)** Box and whisker plot for the proportion of cells in $G_0/G_1$, S, or $G_2$/M phase of the cell cycle following control and $_{HEa}$miRNA overexpression.

**C)** Box and whisker plot for the proportion of cells in $G_0/G_1$, S, or $G_2$/M phase of the cell cycle following control and $_{HEa}$miRNA hairpin inhibitor transfection with or without concomitant 320 mg/dL ethanol exposure.

For box and whisker plots, bounds of box demarcate limits of 1st and 3rd quartile, line in middle is the median, and whiskers represent the range of data. Representative flow cytometry experiment images are shown on the right.

n=10 samples per group; ANOVA: significant main effect of $_{HEa}$miRNA transfection [$^{\#\#}$p<0.01, $^{\#\#\#}$p<0.001, and $^{\#\#\#\#}$p<0.0001]; significant main effect of 320mg/dL ethanol exposure [$^{\varepsilon}$p<0.05]. For post-hoc analysis, *p<0.05 and **p<0.01 by Tukey's HSD.

We sought to determine if pretreating cytotrophoblasts with pooled $_{HEa}$miRNA antagomirs could prevent the cytotrophoblast cell cycle retardation caused by

transfecting $_{HEa}$miRNA mimics. Cells transfected with the control or pooled $_{HEa}$miRNA antagomirs, and subsequently transfected with pooled $_{HEa}$miRNA mimics, did not have significantly different cell cycle profiles or rates of DNA synthesis to each other but had significantly lower rates of DNA synthesis (ANOVA, $F_{(2,12)}$=16.56, p=0.0004), and a decreased proportion of S-phase cells ($F_{(2,12)}$=11.43, p=0.002) with an increased proportion of cells in $G_2$/M phase ($F_{(2,12)}$=11.47, p=0.002), compared to cells transfected with both the control antagomir and control mimic (Figures 16A and B). Collectively, our data indicate that transfection of these antagomirs prevents further reduction in the rate of DNA synthesis, or cell cycle retardation, that would result from transfection with pooled $_{HEa}$miRNA mimics.

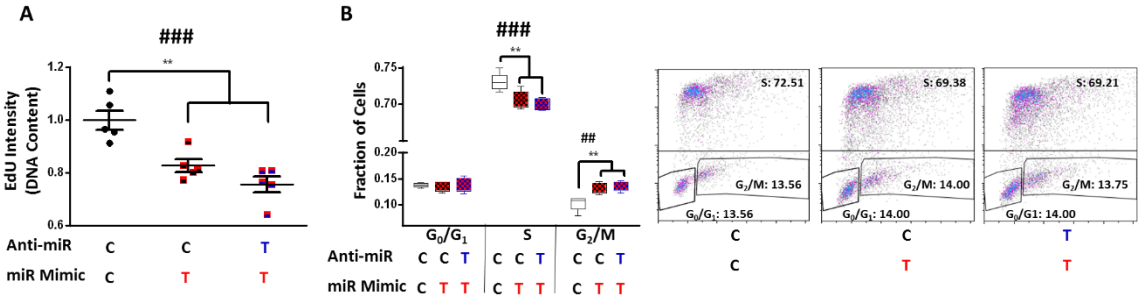


**Figure 16: Antagomirs prevent $_{HEa}$miRNA induced cell cycle retardation**

**A)** Degree of EdU incorporation following control or $_{HEa}$miRNA hairpin inhibitor transfection followed by control or $_{HEa}$miRNA overexpression in BeWO cytotrophoblasts. Results are expressed as expressed as the mean ± SEM.

**B)** Box and whisker plot for the proportion of cells in $G_0/G_1$, S, or $G_2$/M phase of the cell cycle following control or $_{HEa}$miRNA hairpin inhibitor transfection followed by control or $_{HEa}$miRNA overexpression in BeWO cytotrophoblasts. Bounds of box demarcate limits of 1st and 3rd quartile, line in middle is the median, and whiskers represent the range of data. Representative flow cytometry experiment images are shown on the right.

In subheadings: **C** denotes control miRNA mimic or hairpin whereas **T** denotes $_{HEa}$miRNA mimic or hairpin inhibitor. n=5 samples per group; ANOVA: significant treatment effect [$^{###}$p<0.001]. For post-hoc analysis, **p<0.01 by Tukey's HSD.

### 3.10 $_{HEa}$miRNAs have minimal effect on cell survival

We next sought to investigate whether ethanol- and $_{HEa}$miRNA-induced changes in cell cycle were related to an increase in cell death. Only the 320 mg/dL dose of ethanol exposure demonstrated a slight, but marginally significant effect, of increasing lytic cell death ($t(18)=2.022$, $p=0.054$), though there was no effect on apoptosis (Figures 17A and B). However, the changes in cell cycle following transfection of individual or pooled $_{HEa}$miRNA mimics were not mirrored by changes in lytic cell death. Nevertheless, two $_{HEa}$miRNAs, hsa-mir-671-5p and hsa-mir-449a, did significantly increase apoptosis (Unpaired t-test, $p<0.05$, FDR correction) (17C and D).

Contrastingly, transfection of 4 $_{HEa}$miRNA antagomirs individually, significantly increased lytic cell death (Unpaired t-test, all $p<0.05$, FDR correction), with the antagomir to hsa-mir-491-3p also increasing apoptotic cell death ($t(14)=3.383$, $p=0.004$, FDR correction, Figure 17C and D). Likewise, transfection of pooled $_{HEa}$miRNA antagomirs increased lytic cell death ($F_{(1,36)}=11.40$, $p=0.002$) but did not cause increased apoptosis, whereas $_{HEa}$miRNA had minimal effects on lytic or apoptotic cell death (Figures 18A-D). Taken together, our data suggest that while ethanol exposure may increase cytotrophoblast death, increased levels of $_{HEa}$miRNAs have minimal effects on cell death, suggesting that their effect on cell cycle and the EMT pathway is independent of any effect on cell survival.

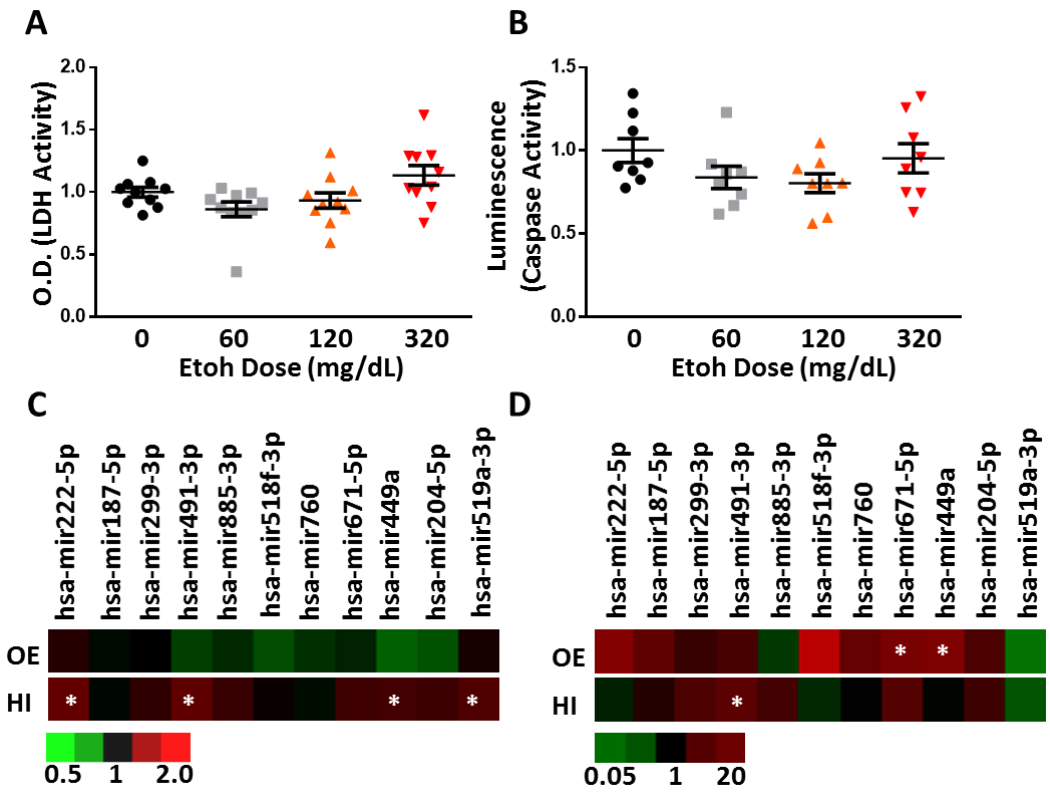


**Figure 17: The effect of ethanol and individual $_{HEa}$miRNAs on lytic and apoptotic cell death**

**A)** Quantification of lytic cell death in BeWO cytotrophoblasts following 0, 60, 120, and 320mg/dL ethanol exposure (n=10 samples per group).

**B)** Quantification of apoptotic cell death in BeWO cytotrophoblasts following 0, 60, 120, and 320mg/dL ethanol exposure (n=8 samples per group).

**C)** Heatmap of lytic cell death in BeWO cytotrophoblasts following individual $_{HEa}$miRNA overexpression (top, OE) or transfection with individual $_{HEa}$miRNA hairpin inhibitors (bottom, HI). Scale for heatmap coloration, bottom, denotes fold change of lytic cell death relative to control mimic or hairpin transfection. N=10 samples per group, white asterisks denote $_{HEa}$miRNA mimics or hairpin inhibitors that had a significant effect, $p<0.05$, Student's t-test, on lytic cell death.

**D)** Heatmap of apoptotic cell death in BeWO cytotrophoblasts following individual $_{HEa}$miRNA overexpression (top, OE) or transfection with individual $_{HEa}$miRNA hairpin inhibitors (bottom, HI). Scale for heatmap coloration, bottom, denotes fold change of apoptotic cell death relative to control mimic or hairpin transfection. N=10 samples per group, white asterisks denote $_{HEa}$miRNA mimics or hairpin inhibitors that had a significant effect, $p<0.05$, Student's t-test, on apoptosis.

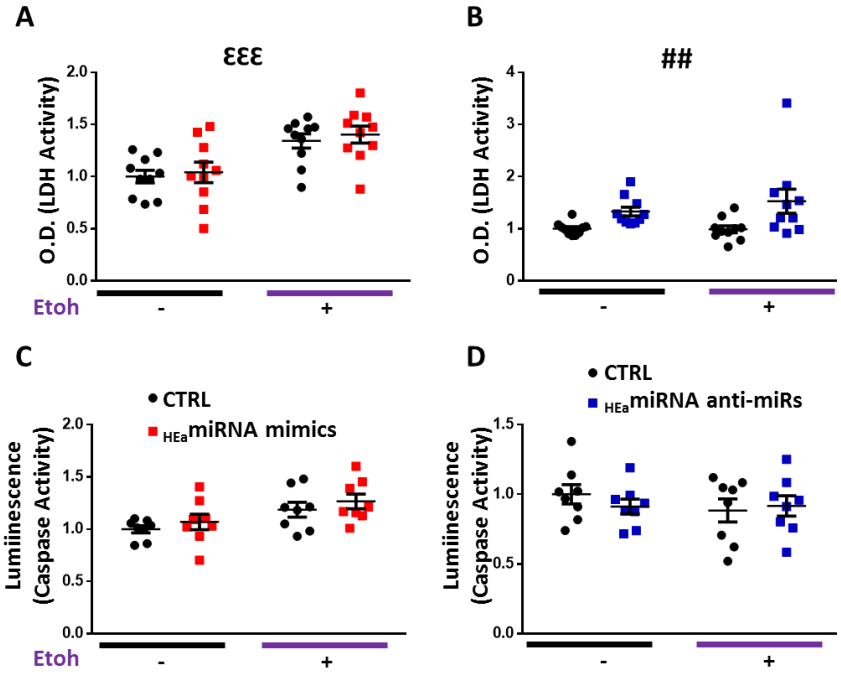


**Figure 18: $_{HEa}$miRNAs influence lytic and apoptotic cell death**

**A)** Quantification of lytic cell death in BeWO cytotrophoblasts following $_{HEa}$miRNAs or control miRNA overexpression with or without concomitant 320mg/dL ethanol exposure (n=10 samples per group).

**B)** Quantification of lytic cell death in BeWO cytotrophoblasts following transfection with $_{HEa}$miRNA or control hairpin inhibitors with or without concomitant 320mg/dL ethanol exposure (n=10 samples per group).

**C)** Quantification of apoptotic cell death in BeWO cytotrophoblasts following $_{HEa}$miRNA mimics or control miRNA overexpression with or without concomitant 320mg/dL ethanol exposure (n=10 samples per group).

**D)** Quantification of apoptotic cell death in BeWO cytotrophoblasts following transfection with $_{HEa}$miRNA or control hairpin inhibitors with or without concomitant 320mg/dL ethanol exposure (n=10 samples per group).

Results are expressed as expressed as the mean ± SEM; ANOVA: significant main effect of 320mg/dL ethanol exposure [$^{\varepsilon\varepsilon\varepsilon}$p<0.001], significant main effect of $_{HEa}$miRNA treatment [$^{\#\#}$p<0.01].

### 3.11 $_{HEa}$miRNAs modulate cytotrophoblast differentiation-associated $Ca^{2+}$ dynamics

$_{HEa}$miRNAs' effects on EMT pathway member expression, coupled with cell cycle retardation, indicates that $_{HEa}$miRNAs influence trophoblast maturation. Maturation of cytotrophoblasts into syncytiotrophoblasts is marked by dramatic changes in the cellular energetics profile (74). To model $_{HEa}$miRNAs' effect on hormone-

producing syncytiotrophoblasts, we used a well-established protocol of forskolin induced syncytialization of BeWO cytotrophoblasts (75, 76). As expected, forskolin treatment induced fusion/syncytialization of cytotrophoblasts resulting in a greater average cell size in the forskolin + $_{HEa}$miRNA mimics group ($F_{(1,386)}$=4.386, p=0.037). This suggests that the inhibition of EMT by these miRNAs may result in preferential syncytialization instead of differentiation to extravillous trophoblasts (Figure 19).

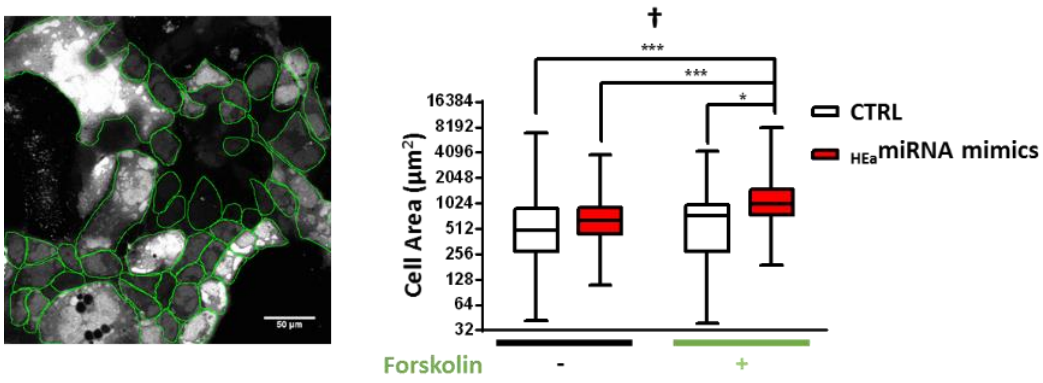


**Figure 19: $_{HEa}$miRNAs promote syncytialization-dependent increases in cell size**
Box and whisker plot of BeWO cytotrophoblast size (left) following $_{HEa}$miRNA overexpression with or without 20µm forskolin treatment. For box and whisker plots, bounds of box demarcate limits of 1st and 3rd quartile, line in middle is the median, and whiskers represent the range of data; ANOVA: significant interaction effect (sex by PAE, [†p<0.05]). For post-hoc analysis, *p<0.05 and ***p<0.001 by Tukey's HSD.

Ethanol and forskolin treatment both increased baseline calcium levels, as indicated by the change in fluo-4 fluorescence ($F_{(1,426)}$=5.593 and 3.665 respectively, p<0.0001, Figures 20A-D). The effect of ethanol on baseline calcium was abrogated by $_{HEa}$miRNAs while $_{HEa}$miRNAs + forskolin was not significantly different to forskolin alone, indicating that forskolin and $_{HEa}$miRNAs may be affecting similar calcium pathways. Syncytiotrophoblasts actively transport high amounts of calcium from maternal to fetal circulation, therefore forskolin-exposed trophoblasts likely have higher

basal transport of calcium into the cells due to increased expression of plasma membrane channels (77). The conversion of trophoblasts to syncytiotrophoblasts is accompanied by an increase in endoplasmic reticulum, which could increase calcium buffering capabilities in response to ethanol-stress on the cells, thus $_{HEa}$miRNA-induced syncytialization pathways may be protective against ethanol stress.

Adaptations to cellular stress can be seen in alterations to cellular energetics in response to ethanol, as ethanol-exposed BeWO cells showed decreased baseline and stressed oxygen consumption rates (OCR) ($F_{(1,28)}$=15.55 and 16.91, p=0.0005 and 0.0003 respectively) and increased extracellular acidification rates (ECAR) ($F_{(1,28)}$=4.868, p=0.036). However, $_{HEa}$miRNAs had minimal effects on metabolic activity (Figures 21A-D).

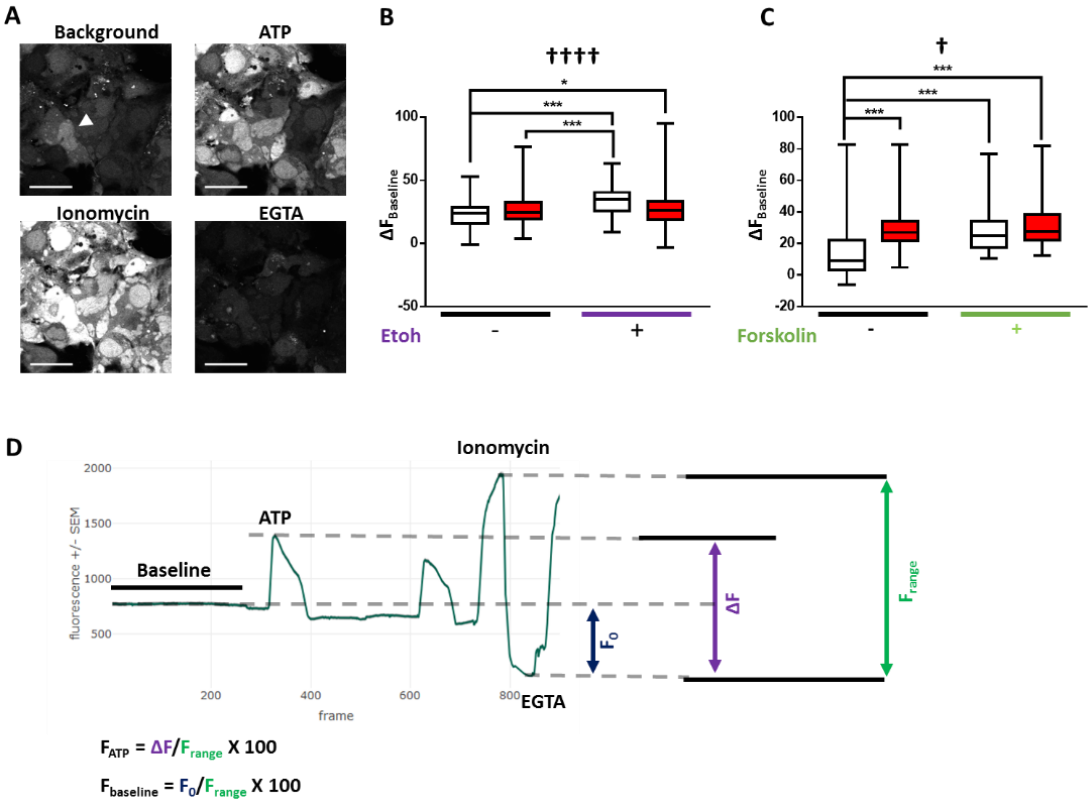


**Figure 20: $_{HEa}$miRNAs influence differentiation associated $Ca^{2+}$ dynamics**

**A)** Time-lapse confocal images of BeWO cytotrophoblasts loaded with fluo-4 $Ca^{2+}$ indicator dye under indicated treatment conditions. Arrowhead indicates a fused, multinuclear cell, scale bar is 50µm.
**B)** Box and whisker plot baseline intracellular calcium levels in BeWO cytotrophoblasts with control and $_{HEa}$miRNA overexpression with or without concomitant 320mg/dL ethanol exposure (n=69 to 154 samples per group).
**C)** Box and whisker plot of baseline intracellular calcium levels in BeWO cytotrophoblasts with control and $_{HEa}$miRNA overexpression with or without 20µm forskolin treatment (n=51 to 136 samples per group).
**D)** Trace of Intracellular Calcium Levels at baseline and following administration of the indicated compounds, as well as schematic and equations used to calculate relative fluorescence intensities (n=51-136 cells per group).

For box and whisker plots, bounds of box demarcate limits of 1$^{st}$ and 3$^{rd}$ quartile, line in middle is the median, and whiskers represent the range of data; ANOVA: significant interaction effect (sex by PAE, [$^{\dagger}$p<0.05, $^{\dagger\dagger\dagger\dagger}$p<0.0001]). For post-hoc analysis, *p<0.05 and ***p<0.001 by Tukey's HSD.

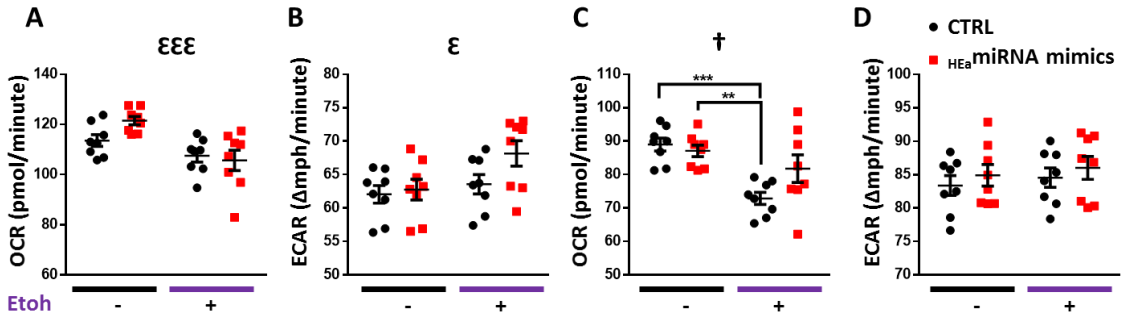


**Figure 21: $_{HEa}$miRNAs have minimal effects on trophoblast metabolism**

**A)** Baseline oxygen consumption rate (OCR), **B)** baseline extracellular acidification rate (ECAR), **C)** stressed OCR, and **D)** stressed ECAR in BeWO cytotrophoblasts with control and $_{HEa}$miRNA overexpression with or without concomitant 320mg/dL ethanol exposure. Metabolic stress was induced by treatment with 1μm Oligomycin and 0.125μM (FCCP). Results are expressed as expressed as the mean ± SEM.

n=10 samples per group; ANOVA: significant main effect of 320mg/dL ethanol exposure [$^{\varepsilon}p<0.05$, $^{\varepsilon\varepsilon\varepsilon}p<0.001$], significant interaction effect ($_{HEa}$miRNA by 320mg/dL ethanol, [$^{\dagger}p<0.05$]). For post-hoc analysis, **p<0.01, ***p<0.001, and ***p<0.0001 by Tukey's HSD.

Extracellular adenosine triphosphate (ATP) has been shown to inhibit trophoblast migration (78) and can directly stimulate increased intracellular calcium elevations through purinergic receptors ubiquitously present on trophoblasts (79). Both $_{HEa}$miRNA and ethanol administration significantly increased intracellular calcium in response to acute ATP administration ($F_{(1,426)}=10.34$ and $F_{(1,386)}=16.30$, $p=0.001$ and $p<0.0001$ respectively) (Figure 22A). This may be indicative of a lack of downregulation of purinergic receptors required in trophoblast migration as part of the interrupted EMT pathway. Forskolin-induced maturation decreased calcium response to ATP ($F_{(1,386)}=50.72$, $p<0.0001$) (Figure 22B) and prevented the $_{HEa}$miRNA-induced increase in ATP response. These data agree with previous studies showing increased nuclear trafficking of ionotropic receptor P2X7 and more localized P2X4 expression over

placental development, which may decrease the overall calcium influx in response to ATP (80).

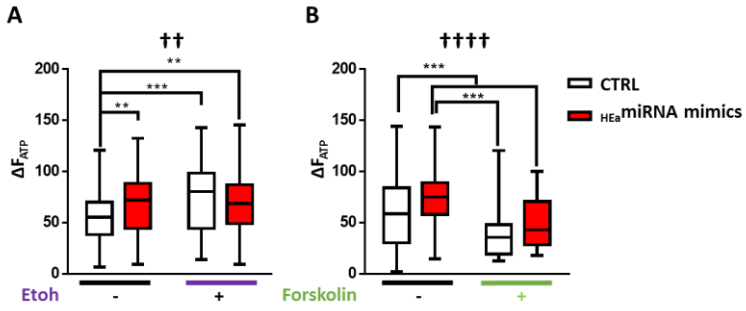


**Figure 22: $_{HEa}$miRNAs influence ATP-exposure associated $Ca^{2+}$ dynamics**
**A)** Box and whisker plot of intracellular calcium levels following acute ATP administration in BeWO cytotrophoblasts with control and $_{HEa}$miRNA overexpression with or without concomitant 320 mg/dL ethanol exposure. Bounds of box demarcate limits of 1st and 3rd quartile, line in middle is the median, and whiskers represent the range of data.
**B)** Box and whisker plot of intracellular calcium levels following acute ATP administration in BeWO cytotrophoblasts with control and $_{HEa}$miRNA overexpression with or without 20 μm forskolin treatment. n=10 samples per group; ANOVA: significant interaction effect ($_{HEa}$miRNA by 320mg/dL ethanol, [$^{††}p<0.01$, and $^{††††}p<0.0001$]). For post-hoc analysis, **p<0.01 and ***p<0.001 by Tukey's HSD.

### 3.12 $_{HEa}$miRNAs promotes syncytialization-dependent hormone production

Transfection of $_{HEa}$miRNA mimics did not change *CGA*, *CGB*, or *IGF2* transcript expression relative to the control in non-syncytialized trophoblasts. However, following syncytialization (Figure 23A), $_{HEa}$miRNA mimics significantly increased expression of *CGA* and *CGB* (post-hoc Tukey's HSD, n=10 samples per group, p=0.001 and 0.005 respectively). Consistent with our previous results, $_{HEa}$miRNA mimics also increased *CDH1* expression in both cytotrophoblasts and syncytiotrophoblasts ($F_{(1,20)}$=5.286, p=0.032); there was also a main effect of syncytialization on *CDH1* expression, as has been previously reported ($F_{(1,36)}$=3.391, p=0.034, Figures 23B-E). Likewise, $_{HEa}$miRNAs increased E-cadherin protein expression ($F_{(1,20)}$=5.286, p=0.032), whereas forskolin

decreased it ($F_{(1,20)}$=10.24, p=0.005) (Figure 23F). On the other hand, there was no effect of $_{HEa}$miRNA antagomirs on *CGA* and *CGB* expression, although we did observe a decrease in *IGF2* transcript expression, following syncytialization, relative to controls (post-hoc Tukey's HSD, n=10 samples per group, p=0.001) (Figure 23G-J).

Given that $_{HEa}$miRNAs promotes syncytialization-dependent hormone production, we next investigated maternal plasma levels of intact human chorionic gonadotropin (hCG) in our Ukraine birth cohort. Plasma hCG levels were non-significantly increased in the second trimester of HEa group mothers relative to their UE counterparts, consistent with previous studies (81). During the third trimester, however, hCG levels remained significantly elevated in HEa group mothers compared to the UE group (Median Test, n=23 samples in HEa group and n=22 for HEua and HEa groups, p=0.03) (Figure 24A). Furthermore, there was no significant difference of gestational age at blood draw between the different groups indicating the increased level of hCG in the HEa group was not confounded by gestational age at which blood was sampled (Figure 24B) (82). Interestingly, both alcohol and hCG levels were negatively associated with gestational age at delivery (GAD), with a significant interaction between periconceptional alcohol exposure and hCG levels on GAD (Table 4). Taken together, our data suggests $_{HEa}$miRNAs may contribute to PAE-dependent increases in hCG levels during pregnancy.

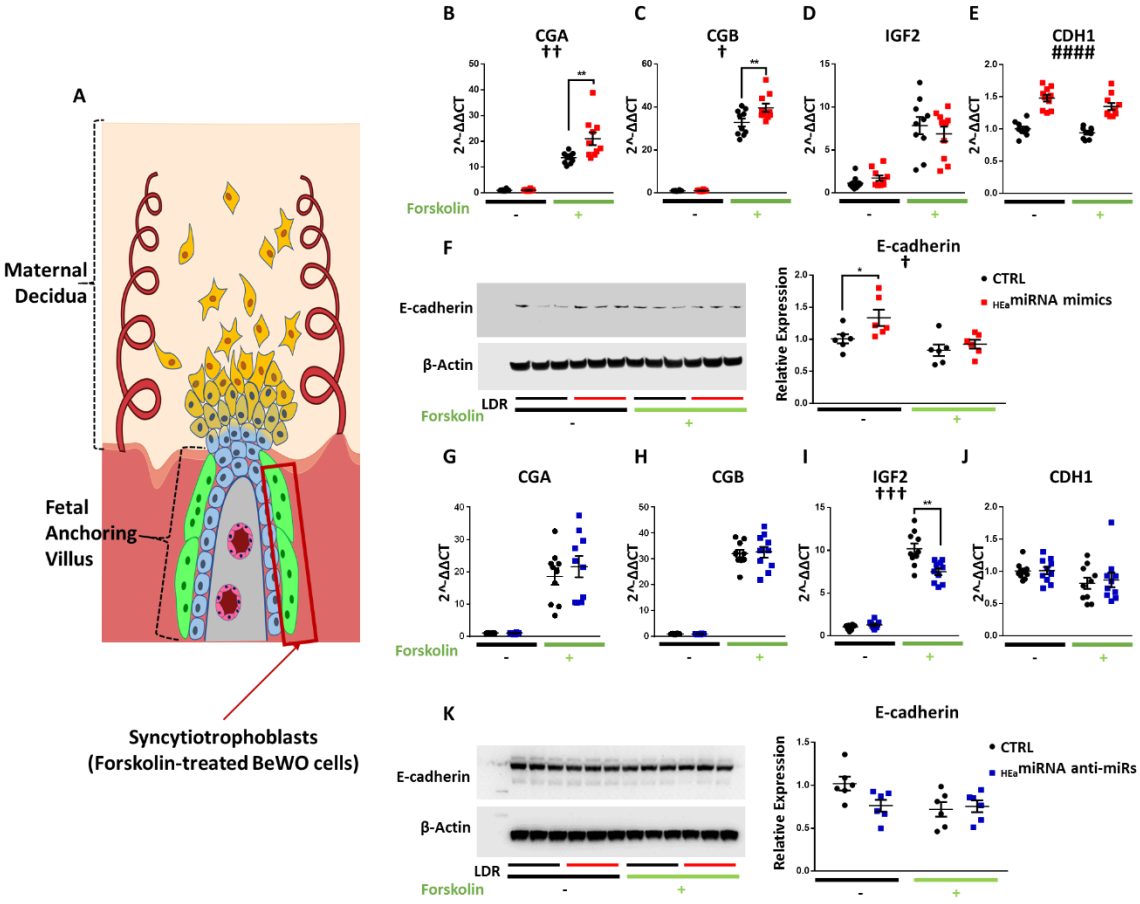


**Figure 23: $_{HEa}$miRNAs promote syncytialization dependent hCG production**
**A)** Diagram of a placental anchoring villous and maternal decidua with the boxed area denoting syncytiotrophoblasts.
Expression of **B)** *CGA*, **C)** *CGB*, **D)** *IGF2*, and **E)** *CDH1* transcripts **F)** and densitometric quantification of E-cadherin protein levels in BeWO cytotrophoblasts following $_{HEa}$miRNAs or control miRNA overexpression with or without 20 μm forskolin treatment.
Expression of **G)** *CGA*, **H)** *CGB*, **I)** *IGF2*, and **J)** *CDH1* transcripts **K)** and densitometric quantification of E-cadherin protein levels in BeWO cytotrophoblasts following $_{HEa}$miRNAs or control hairpin inhibitor transfection with or without 20 μm forskolin treatment.
Results are expressed as expressed as the mean ± SEM, LDR=Molecular Weight Ladder, n=10 samples per group; ANOVA: significant main effect of $_{HEa}$miRNA transfection [$^{####}$p<0.0001], significant interaction effect ($_{HEa}$miRNA by 320mg/dL ethanol, [$^{\dagger}$p<0.05]). For post-hoc analysis, *p<0.05, **p<0.01 by Tukey's HSD.

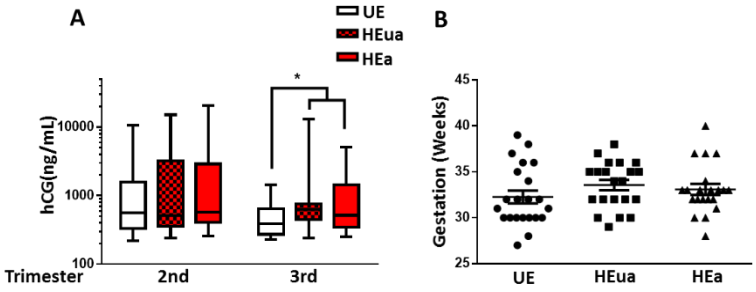


**Figure 24: PAE elevates 3rd trimester maternal hCG**

A) Box and whisker plot of 2nd and 3rd trimester maternal hCG levels in UE, HEua, and HEa group mothers of our Ukrainian birth cohort. Bounds of box demarcate limits of 1st and 3rd quartile, line in middle is the median, and whiskers represent the range of data.
B) Gestational age at third-trimester maternal blood collection across the UE, HEua, and HEa groups within our Ukrainian birth cohort n=22-23 samples per group; *p=0.03 (Mood's Median Test, $\chi^2$=7.043, df=2).

## 3.13 HEamiRNAs reduce fetal growth

To investigate the functional consequences of elevated circulating HEamiRNA levels, we administered miRNA mimics for the 8-mouse homologue HEamiRNAs, or a negative control mimic, through tail-vein injection to pregnant mouse dams on GD10. On GD18, growth parameters of male and female fetuses were assessed separately (Figure 25A), and data from all same-sex fetuses from a single pregnancy were averaged into one data point. Dams administered HEamiRNA mimics produced smaller fetuses than those administered control mimics, according to all collected measures of fetal size: fetal weight ($F_{(1,17)}$=9.92, p=0.006), crown-rump length ($F_{(1,17)}$=9.89, p=0.006), snout-occipital distance ($F_{(1,17)}$=9.09, p=0.008), and biparietal diameter ($F_{(1,17)}$=5.99, p=0.026) (Figure 25B-E). Interestingly, placental weights were also significantly reduced in mice treated with HEamiRNA mimics ($F_{(1,17)}$=6.92, p=0.018) (Figure 25F).

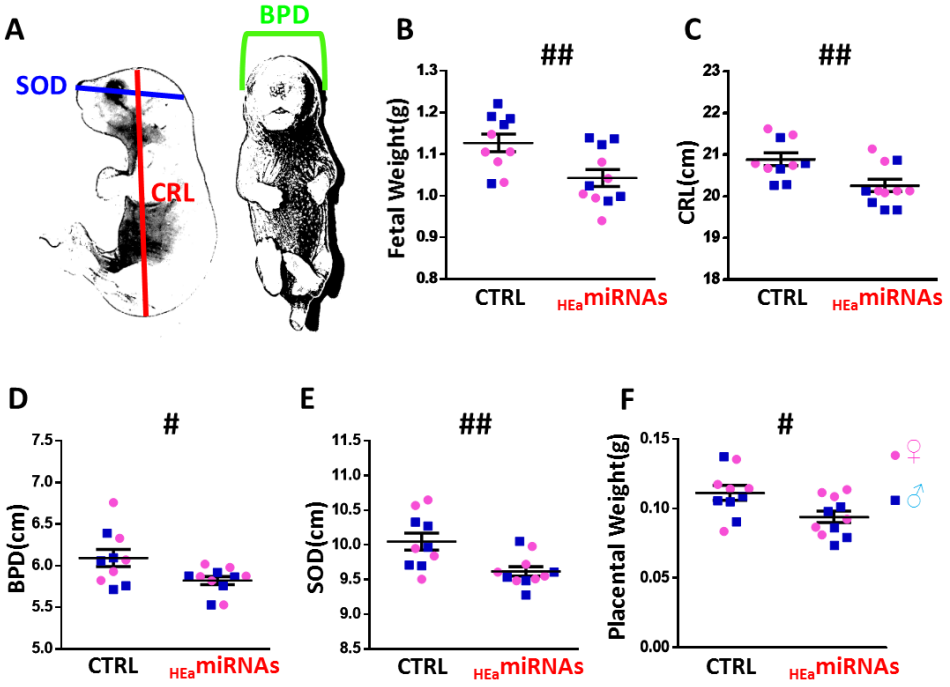


**Figure 25: $_{HEa}$miRNAs restrict fetal growth**

**A)** Schematic for measures of crown rump length (CRL), biparietal diameter (BPD), and snout-occipital distance (SOD).

**B)** Fetal weight, **C)** crown-rump length, **D)** biparietal diameter, **E)** snout-occipital distance, **F)** and placental weight at GD18 following administration of control (Ctrl) and $_{HEa}$miRNA mimics to pregnant C57/Bl6 dams on GD10. Dots represent median measures of fetal size and placental weights from male and female offspring in independent litters. There were no significant differences in litter sizes [Ctrl: 8.2 and $_{HEa}$miRNAs: 8.5] or sex ratios [Ctrl: 0.86 and $_{HEa}$miRNAs: 1.21] between treatment conditions ($p>0.5$ for all measures).

Results are expressed as expressed as the mean ± SEM, n=5-6 separate litters per treatment condition; ANOVA: significant main effect of $_{HEa}$miRNA administration [$^{\#}p<0.05$ and $^{\#\#}p<0.01$].

Following tail-vein administration of two human-specific sentinel miRNAs, miR-518f-3p and miR-519a-3p, we found a high biodistribution of both miRNAs in the placenta, comparable to levels seen in the liver and spleen (Figure 26A and B). Thus, to determine whether $_{HEa}$miRNA's effects on fetal growth could result from their actions on the placenta, we quantified the placental expression of core EMT members in the GD18 placentas of control and $_{HEa}$miRNA fetuses. $_{HEa}$miRNA administration significantly

reduced expression of mesenchymal-associated transcript *VIM* ($F_{(1,14)}$=14.23, p=0.002) and S*NAI2* ($F_{(1,14)}$=5.99, p=0.028) with a significant sex by $_{HEa}$miRNA interaction effect on *SNAI1* ($F_{(1,66)}$=5.55, p=0.034) and *CDH1* ($F_{(1,14)}$=6.01, p=0.028) (Figures 27A-E). Interestingly, and in line with our *in vitro* findings whereby $_{HEa}$miRNAs promoted syncytialization dependent cell fusion and hCG production, $_{HEa}$miRNA administration significantly increased expression of the mRNA transcript for *SynB*, a gene that is important for syncytiotrophoblast maturation ($F_{(1,66)}$=4.11, p=0.047) (Figure 27F).

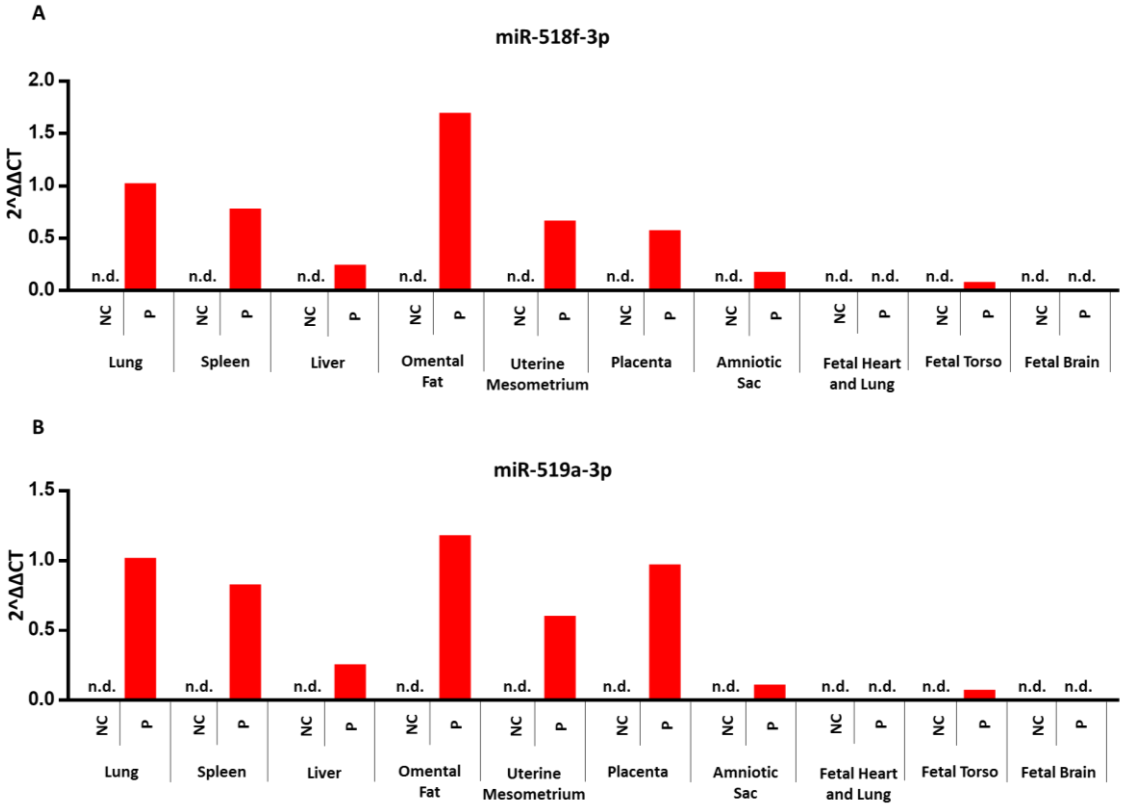


**Figure 26: Biodistribution of miRNAs following systemic administration**
Expression of **A)** miR-518f-3p or **B)** miR-519a-3p in the indicated fetal and maternal compartments at GD12 following tail vein injection of control (NC) and miR-518f-3p or miR-519a-3p mimics (P) to pregnant C57/Bl6 dams on GD10.
n=1 sample per group, n.d. indicates non-detectable levels of miRNA.

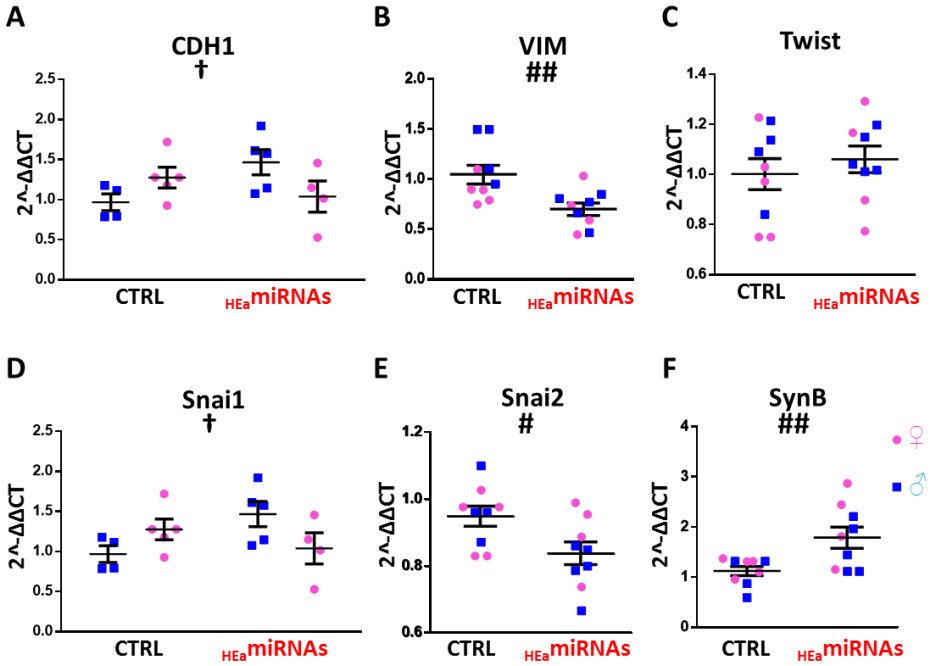


**Figure 27: $_{HEa}$miRNAs interfere with EMT in the placenta**

Expression of **A)** *CDH1* **B)** *VIM* **C)** *TWIST* **D)** *SNAI1* and **E)** *Snai2* and **F)** *SynB* transcripts in GD18 placenta following administration of control (Ctrl) and $_{HEa}$miRNA mimics to pregnant C57/Bl6 dams on GD10.

Dots represent median expression values of male and female offspring in independent litters. Results are expressed as expressed as the mean ± SEM, n=5-6 separate litters per treatment condition, ANOVA: significant main effect of $_{HEa}$miRNA administration [$^{\#}p<0.05$, $^{\#\#\#}p<0.001$], significant interaction effect (fetal sex by $_{HEa}$miRNA administration, [$^{\dagger}p<0.05$]). For post-hoc analysis, $^{*}p<0.05$ by Tukey's HSD.

### 3.14 $_{HEa}$miRNAs reduce placental-directed blood flow

Given the profound effects of $_{HEa}$miRNA administration on inhibiting fetal and placental growth as well as placental EMT, we next decided to characterize their effects on blood-flow dynamics at the maternal-fetal interface (Figure 28). Interestingly, we found that fetuses of $_{HEa}$miRNA treated dams had a non-significantly reduced pulsatile acceleration in the uterine arteries compared to those from control treated dams at GD18 (Figure 29A). Furthermore, $_{HEa}$miRNA treatment also produced marginally significantly reductions in mean and peak blood flow velocity in the umbilical arteries (Unpaired t-

test, p=0.089 and 0.092 respectively), and a significantly reduced blood flow velocity time integral (Unpaired t-test, 0=0.031) (Figures 29B-D). There was also a non-significant trend towards reduced pulsatile acceleration in the ascending aorta (Unpaired t-test, p=0.032) while there was no effect on flow velocities within the ascending aorta (Figures 29E-H).

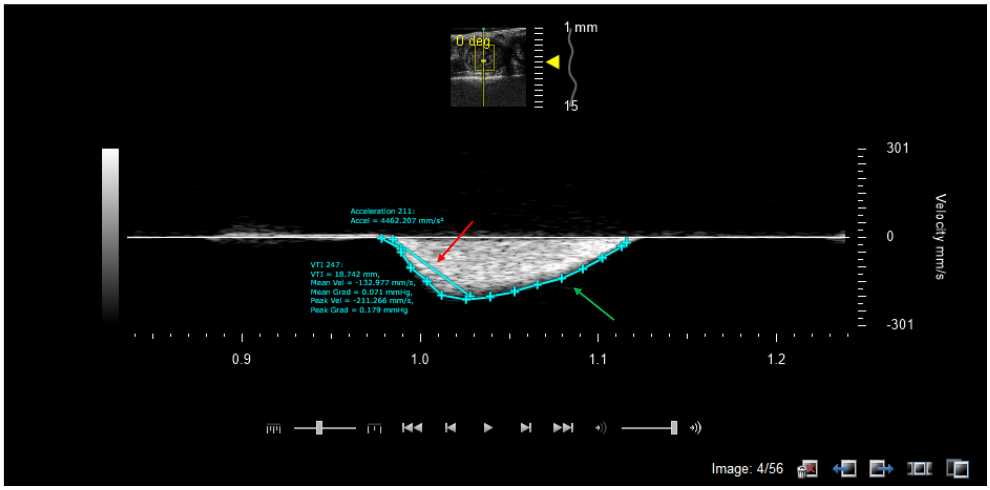


**Figure 28: Tracing of fetal blood flow dynamics**
Ultrasound measurement of blood flow velocity and acceleration on ascending aorta of GD12 fetus. Red arrow demarcates blood flow acceleration measured from beginning of reading to peak. Green arrow demarcates blood flow velocity measured by tracing the parameter of measurement curve. Imaging and measurements of blood-flow dynamics were taken repeatedly for each pregnant dam on GD12, GD14 and GD18 for both the umbilical and ascending arteries for a fetus in the upper left and upper right quadrant of the uterine horn.

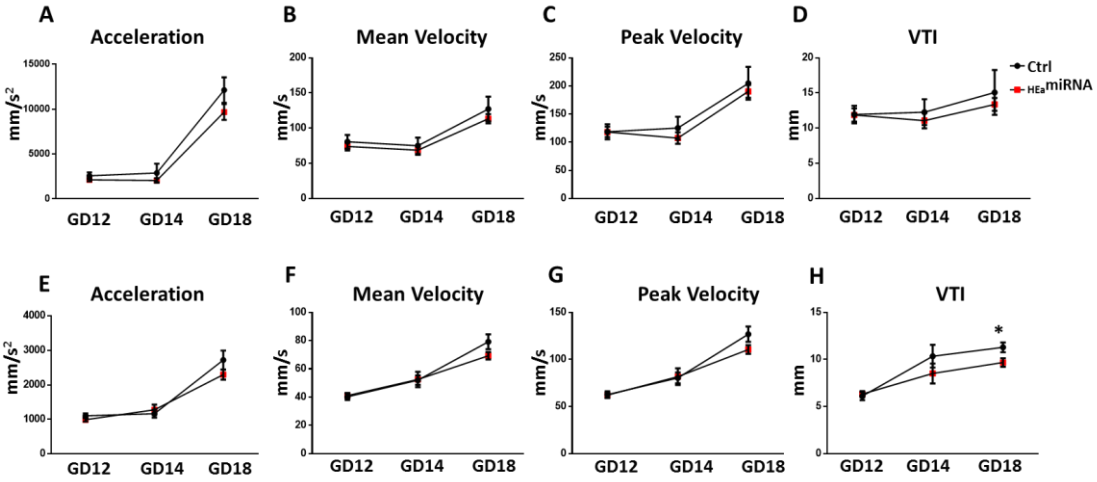


**Figure 29: Effects of $_{HEa}$miRNAs on mouse model umbilical and fetal blood flow dynamics**
A) Pulsatile acceleration, B) mean blood flow velocity, C) Peak blood flow velocity, and D) Velocity Time Integral in the fetal ascending aorta.
E) Pulsatile acceleration, F) mean blood flow velocity, G) Peak blood flow velocity, and H) Velocity Time Integral in the umbilical aorta.
n=10 samples per group, *p<0.05 by Unpaired t-test

**Table 1: List of primer sequences used**

| Target | Forward Sequence | Reverse Sequence | Product Size | NCBI Accession Number |
|---|---|---|---|---|
| Homo_sapien Snai1 | CGAGTGGTTCTTCTGCGCTA | CTGCTGGAAGGTAAACTCTGGA | 157bp | NM_005985 |
| Homo_sapien Snai2 | GAACTGGACACACATACAGTGAT | ACTCACTCGCCCCAAAGATG | 201bp | NM_003068 |
| Homo_sapien Twist | ATTCAGACCCTCAAGCTGGC | TTCTCTGGAAACAATGACATCTAGG | 236bp | NM_000474 |
| Homo_sapien CDH1 | GTACAACGACCCAACCCAAGA | CTCTTTGACCACCGCTCTCC | 212bp | NM_004360 |
| Homo_sapien VIM | CGGGAGAAATTGCAGGAGGA | AAGGTCAAGACGTGCCAGAG | 105bp | NM_003380 |
| Homo_sapien HPRT | CCCTGGCGTCGTGATTAGTG | TCGAGCAAGACGTTCAGTCC | 139bp | NM_000194 |
| Homo_sapien ACTB | CCATCCTGCGTCTGGACCT | TCCATGCCCAGGAAGGAAGG | 289bp | NM_001101 |
| Homo_sapien 18s | ATGGCCGTTCTTAGTTGGTG | CGCTGAGCCAGTCAGTGTAG | 217bp | K03432 |
| Homo_sapien CGA | CCAGAATGCACGCTACAGGA | CCCCATTACTGTGACCCTGTT | 195bp | NM_001252383 |
| Homo_sapien CGB | GGACATGGGCATCCAAGGAG | CACGCGGGTCATGGTGG | 143bp | NM_033043 |
| Homo_sapien IGF2 | CGGCTTCTACTTCAGCAGG | GGAAACAGCACTCCTCAACG | 74bp | NM_000612 |
| Mus_musculus Snai1 | GCGGAGTTGACTACCGACC | GAAGGTGAACTCCACACACG | 275bp | NM_011427 |
| Mus_musculus Snai2 | ACTGGACACACACACAGTTATT | CTGCCGACGATGTCCATACA | 128bp | NM_011415 |
| Mus_musculus Twist | CTCGGACAAGCTGAGCAAGA | ATGACATCTAGGTCTCCGGC | 240bp | NM_011658 |
| Mus_musculus CDH1 | TCGCCACAGATGATGGTTCA | CTCAGCAGTAAAGGGGGACG | 191bp | NM_009864 |
| Mus_musculus VIM | GACCAGAGATGGACAGGTGA | ACGTCTTTTGGGGTGTCAGT | 225bp | NM_011701 |
| Mus_musculus SynB | ACACCCTCATTAAACAGGTTCTC | AGGTCCCTTTCCGGAAGACT | 208bp | NM_173420 |
| Mus_musculus 18s | ATGGCCGTTCTTAGTTGGTG | CGCTGAGCCAGTCAGTGTAG | 217bp | NR_003278 |
| Mus_musculus HPRT | AGTCCCAGCGTCGTGATTAG | TGATGGCCTCCCATCTCCTT | 170bp | NM_013556 |
| Mus_musculus ACTB | CTCTGGCTCCTAGCACCATGAAGA | GTAAAACGCAGCTCAGTAACAGTCCG | 200bp | NM_007393 |
| Rattus_Norvegicus CDH1 | CTGGGGTCATCAGTGTGGTC | TTGACCCTGGTACGTGCTTG | 182bp | NM_031334 |
| Rattus_Norvegicus VIM | TGCGAGAAAAATTGCAGGAGG | AGGCTTGGAAACGTCCACAT | 236bp | NM_031140 |
| Rattus_Norvegicus Snai1 | AGCAGAGTTGTCTACCGACC | GGAAGGTGAACTCCACACAC | 159bp | NM_053805 |
| Rattus_Norvegicus Snai2 | CACATTCGGACCCACACGTT | GCTTTTCCCCAGTGTGTGTTCT | 106bp | NM_013035 |
| Rattus_Norvegicus Twist | CGGAGACCTAGATGTCATTGTT | GCAGAGGTGTGAGGGTGATG | 231bp | NM_053530 |
| Rattus_Norvegicus ACTB | AGATCAAGATCATTGCTCCTCCT | ACGCAGCTCAGTAACAGTCC | 174bp | NM_031144 |
| Rattus_Norvegicus 18s | ATGGCCGTTCTTAGTTGGTG | CGCTGAGCCAGTCAGTGTAG | 217bp | NR_046237 |

**Table 2: $_{HEa}$miRNAs are significantly correlated with independent measures of infant size**
The correlation of 2nd and 3rd trimester maternal plasma $_{HEa}$miRNA levels with independent measures of infant size. $_{HEa}$miRNAs and their significantly correlated sex and gestational age-adjusted growth parameters appear in bold. *p<0.05, **p<0.01.

| | | Weight | | | Height | | | Head Circumference | | |
|---|---|---|---|---|---|---|---|---|---|---|
| MIMAT # | Trimester | Sig. | $R^2$ | ρ | Sig. | $R^2$ | ρ | Sig. | $R^2$ | ρ |
| MIMAT0004569 | 2 | 0.821 | 1.224 | -0.051 | 0.066 | 9.572 | -0.179 | 0.8 | 1.732 | -0.104 |
| MIMAT0004561 | 2 | 0.462 | 6.347 | 0.068 | 0.17 | 12.607 | -0.074 | 0.134 | 10.903 | 0.103 |
| **MIMAT0000687** | 2 | 0.552 | 1.113 | 0.029 | 0.069 | 9.299 | -0.203 | **0.036*** | **8.65** | **0.1** |
| **MIMAT0004765** | 2 | 0.172 | 3.61 | 0.112 | 0.849 | 2.033 | -0.055 | **0.024*** | **12.529** | **0.156** |
| **MIMAT0004948** | 2 | 0.142 | 4.227 | -0.174 | **0.044*** | **7.667** | **-0.231** | 0.59 | 1.36 | -0.115 |
| **MIMAT0002842** | 2 | 0.246 | 2.517 | 0.134 | 0.918 | 2.134 | -0.118 | **0.007**** | **14.561** | **0.219** |
| MIMAT0004957 | 2 | 0.059 | 6.314 | 0.195 | 0.22 | 4.096 | 0.079 | 0.055 | 10.158 | 0.195 |
| MIMAT0003880 | 2 | 0.123 | 7.24 | 0.11 | 0.578 | 5.264 | -0.031 | 0.073 | 10.794 | 0.107 |
| MIMAT0001541 | 2 | 0.101 | 11.584 | 0.104 | 0.718 | 5.851 | -0.072 | 0.173 | 10.036 | 0.068 |
| **MIMAT0000265** | 2 | **0.026*** | **12.377** | **0.184** | 0.272 | 4.973 | 0 | 0.131 | 7.095 | 0.108 |
| **MIMAT0002869** | 2 | **0.034*** | **7.975** | **0.153** | 0.403 | 6.83 | -0.012 | 0.093 | 8.181 | 0.096 |
| **MIMAT0004569** | 3 | 0.875 | 0.993 | -0.046 | **0.018*** | **10.709** | **-0.196** | 0.577 | 4.696 | -0.01 |
| MIMAT0004561 | 3 | 0.538 | 2.055 | 0.049 | 0.37 | 2.029 | -0.109 | 0.784 | 3.697 | 0.002 |
| MIMAT0000687 | 3 | 0.511 | 0.762 | 0.005 | 0.514 | 1.769 | -0.072 | 0.87 | 3.786 | -0.077 |
| MIMAT0004765 | 3 | 0.824 | 3.165 | -0.028 | 0.2 | 12.122 | -0.121 | 0.747 | 4.188 | -0.081 |
| MIMAT0004948 | 3 | 0.807 | 0.148 | 0.029 | 0.102 | 4.686 | -0.156 | 0.376 | 5.009 | 0.032 |
| MIMAT0002842 | 3 | 0.515 | 2.099 | 0.109 | 0.421 | 1.715 | 0.016 | 0.245 | 7.917 | 0.152 |
| MIMAT0004957 | 3 | 0.368 | 1.396 | 0.141 | 0.761 | 0.716 | -0.022 | 0.207 | 6.052 | 0.172 |
| MIMAT0003880 | 3 | 0.055 | 8.715 | 0.155 | 0.367 | 3.521 | -0.133 | 0.076 | 8.196 | 0.15 |
| **MIMAT0001541** | 3 | 0.995 | 0.085 | -0.06 | 0.982 | 0.678 | -0.151 | **0.026*** | **12.022** | **0.135** |
| **MIMAT0000265** | 3 | **0.019*** | **11.872** | **0.23** | 0.206 | 5.589 | 0.022 | **0.002**** | **18.683** | **0.319** |
| MIMAT0002869 | 3 | 0.391 | 2.82 | 0.043 | 0.302 | 5.917 | -0.151 | 0.106 | 9.286 | 0.118 |

**Table 3: $_{HEa}$miRNAs collectively explain the variance in independent measures of infant size**
$R^2$ values resulting from a multivariate statistical regression model for 2$^{nd}$ and 3$^{rd}$ trimester $_{HEa}$miRNA levels fit onto sex and gestational-age adjusted growth parameters.

| | 2$^{nd}$ Trimester $R^2$ | 3$^{rd}$ Trimester $R^2$ |
|---|---|---|
| Weight | 24.983 | 13.303 |
| Height | 24.568 | 13.505 |
| Head Circumference | 31.844 | 28.675 |

**Table 4: Maternal alcohol consumption and hCG levels are negatively correlated with gestational age at delivery**

| | Estimate | C.I. | Sig. |
|---|---|---|---|
| **AAD0** | | | |
| (Intercept) | 39.37 | (31.41, 47.33) | <.001*** |
| AAD0 | -8.71 | (-15.98, -1.43) | 0.020* |
| hCG Level (log) | -0.87 | (-1.7, -0.03) | 0.042* |
| Gestational Age at Blood Draw | 0.18 | (0.02, 0.33) | 0.028* |
| AAD0:hCG Level (Interaction) | 1.2 | (0.05, 2.35) | 0.040* |
| **AADD0** | | | |
| (Intercept) | 38.42 | (30.55, 46.28) | <.001*** |
| AAD0 | -2.65 | (-6.3, 1.01) | 0.153 |
| hCG Level (log) | -0.7 | (-1.63, 0.23) | 0.137 |
| Gestational Age at Blood Draw | 0.17 | (0.02, 0.33) | 0.028* |
| AADD0:hCG Level (Interaction) | 0.36 | (-0.22, 0.94) | 0.222 |
| **AADXP** | | | |
| (Intercept) | 38.22 | (32.01, 44.44) | <.001*** |
| AADXP | -31.84 | (-69.34, 5.67) | 0.095 |
| hCG Level (log) | -0.57 | (-1.13, 0) | 0.049* |
| Gestational Age at Blood Draw | 0.15 | (0, 0.3) | 0.052 |
| AADXP:hCG Level (Interaction) | 4.54 | (-1.86, 10.93) | 0.161 |
| **AADDXP** | | | |
| (Intercept) | 37.96 | (31.85, 44.07) | <.001*** |
| AADDXP | -2.67 | (-10.08, 4.73) | 0.473 |
| hCG Level (log) | -0.49 | (-1.05, 0.07) | 0.085 |
| Gestational Age at Blood Draw | 0.15 | (0, 0.3) | 0.051 |
| AADDXP:hCG Level (Interaction) | 0.23 | (-1.03, 1.48) | 0.718 |

# 4. DISCUSSION*

In a prior study, we reported that gestational elevation of 11 maternal plasma miRNAs, in a Ukrainian clinical cohort, predicted which PAE infants would exhibit adverse outcomes at birth (11). These $_{HEa}$miRNAs were elevated throughout mid and late-pregnancy, encompassing critical periods for fetal development, and were predicted to target key developmental pathways (11). Given that $_{HEa}$miRNAs are placentally enriched and their dysregulation is associated with placental-associated gestational pathologies, we sought to determine if they also contributed to the pathophysiology of FASDs.

To mimic the alcohol consumption patterns in our Ukrainian cohort, we adopted moderate alcohol self-administration paradigms during mouse and macaque gestation. Though these species share a hemochorial placenta, fundamental differences in placental anatomy remain. Specifically, macaque trophoblasts exhibit deeper invasion into the uterine horn than their mouse counterparts (83-86). Despite these differences, we found PAE inhibited mesenchymal transition-associated mRNA transcripts in both our models, indicating a conserved effect of PAE on placental development. Additionally, we found that $_{HEa}$miRNAs mediated the effects of PAE on core EMT pathway members in the placenta, and collectively though not individually, inhibited EMT in human cytotrophoblast and extravillous trophoblast culture models. The components of the EMT pathway were selected for assessment based on a substantial literature that

* Part of this chapter is reprinted with permission from "Maternal circulating miRNAs that predict infant FASD outcomes influence placental maturation" by Tseng et al., 2019. *Life Science Alliance*, Vol. 2, © 2019 by Tseng et al.

implicates these as core EMT components (13, 17, 18, 67-70). However, analysis of their 3'UTRs indicates that these are unlikely to be the direct targets of $_{HEa}$miRNA action. Additional studies will be needed to dissect out the signaling networks that connect $_{HEa}$miRNAs to the assessed EMT components.

Interestingly, $_{HEa}$miRNAs also promoted syncytialization (forskolin)-dependent hCG expression, mirroring the elevation of third trimester maternal hCG levels in the PAE group within our Ukrainian birth cohort. This late-gestation elevation of hCG levels may serve as a compensatory mechanism to prevent the preterm birth associated with PAE, as hCG during late gestation is hypothesized to promote uterine myometrial quiescence (87, 88). In support of this hypothesis, we found significant negative associations between both hCG levels and alcohol consumption with gestational age at delivery. Furthermore, there was a significant interaction between periconceptional alcohol exposure and hCG levels, with higher hCG levels corresponding to a smaller effect of alcohol exposure at conception on gestational age at delivery, indicating that hCG moderates the effect of alcohol on age at delivery (Table 4).

Since $_{HEa}$miRNAs collectively prevented trophoblast EMT, we hypothesized that, as a functional consequence, these maternal miRNAs would also inhibit fetal growth. When we delivered 8 out of the 11 $_{HEa}$miRNAs known to be present in mouse, to pregnant dams during the period of placental branching morphogenesis and endometrial invasion, when EMT is particularly active, we found that $_{HEa}$miRNAs reduced fetal growth. Importantly, ethanol exposure during this period has also been shown to result in fetal growth deficits and dysmorphia in rodent PAE models (89, 90) suggesting that

maternal miRNA-mediated deficits in trophoblast invasion may mediate some of the effects of PAE on fetal growth. In support of this, we found placentas from the $_{HEa}$miRNA treated group had impaired expression of core EMT pathway members. It is also feasible that $_{HEa}$miRNAs disrupt fetal growth through placental vascular dynamics. Indeed, we observed reduced placentally-directed blood flow in the $_{HEa}$miRNA-treated group compared to controls. Furthermore, the non-human primate tissue analyzed here was derived from animals that were characterized *in vivo* using MRI and ultrasound imaging, which demonstrated that maternal blood supply to the placenta was lower in ethanol-exposed animals compared to controls, and that oxygen availability to the fetal vasculature was reduced (91). Thus, one possibility is that compromised trophoblast invasion contributes to impaired maternal blood flow in ethanol-exposed individuals, as we have also previously observed in mouse models (92).

Impaired nutrient uptake in the placenta, such as dysfunction in the amino acid, glucose, and fatty acid transport systems have also been implicated in gestational pathologies, such as intrauterine growth restriction (93). Furthermore, *in vitro* studies in trophoblasts have shown alcohol exposure selectively impairs a subset of these amino acid and fatty acid transport systems (94, 95) whilst *in vivo*, PAE in rodents alters expression of glucose transporters in the late gestation placenta (23). These placental dysfunctions could also have insidious effects on development that are not immediately detectable at birth. As an example, perturbations in placental iron transport by PAE may impair central nervous system development during the neonatal period, leading to cognitive deficits that last throughout adulthood (96, 97). Thus, further investigation is

warranted to determine if $_{HEa}$miRNAs contribute to this alcohol induced impairment in trans-placental nutrient transport, and ultimately whether this impairment of nutrient transport represents another avenue through which PAE disrupts fetal development.

It is likely that $_{HEa}$miRNAs may mediate other pregnancy associated pathologies, aside from PAE. We identified numerous studies that reported increased circulating and placental levels of at least 8 out of 11 $_{HEa}$miRNAs in gestational pathologies arising from placental dysfunction. For example, elevated levels of one $_{HEa}$miRNA, miR-519a-3p, a member of the placentally-expressed C19MC family cluster, was reported in placentae of patients with pre-eclampsia, recurrent spontaneous abortion, and intrauterine growth restriction (40, 41, 54, 55). Interestingly, collective overexpression of the 59 C19MC miRNAs inhibits trophoblast migration, explaining their enrichment in the non-migratory villous trophoblasts and suggests their downregulation is necessary for maturation into invasive extravillous trophoblasts (98). Thus, a greater understanding of the placental roles of $_{HEa}$miRNAs may also help disentangle the etiology of other pregnancy complications.

While our data suggest that the placenta is an important contributory source for circulating $_{HEa}$miRNAs, the effects of $_{HEa}$miRNAs likely extend beyond the placenta into other maternal tissues. Outside of the placenta, $_{HEa}$miRNAs may circulate in association with lipoprotein complexes, or be encapsulated in extracellular vesicles (EVs) whose abundance dramatically increases during pregnancy (99, 100). Recent work has demonstrated that placental-derived EVs can regulate the maternal immune system as well as confer viral resistance to recipient cells, including endothelial cells (101-104).

Interestingly, other studies also have identified endothelial cells as ready recipients for placental-derived EVs, suggesting placental-EVs and their cargo miRNAs participate in synchronizing the growth of the placenta with the accompanying maternal and fetal vascular remodeling (99, 105). While further investigation is warranted into the role of EVs and miRNAs in maternal-fetal communication, and to the extent they serve as paracrine/endocrine mediators for the placenta during development, targeting $_{HEa}$miRNAs will likely have profound effects for both fetal and placental development in the context of FASDs and other gestational pathologies.

While we did not investigate the effects of PAE on EMT in non-placental organs, it is likely that PAE broadly disrupts EMT in multiple fetal compartments. Developmental ethanol exposure has been shown inhibit the EMT-dependent migration of neural crest progenitors involved in craniofacial development, explaining the facial dysmorphology seen in FAS and FASDs (106, 107). Outside of its effects on the neural crest, PAE is significantly associated with various congenital heart defects, including both septal defects and valvular malformations (108-111). Septation of the heart, primarily atrial septation, is an EMT-dependent process, with endocardial cells delaminating and transdifferentiating into mesenchymal cells that populate the endocardial cushions as well as the muscular cap, which functions as the growing edge of the muscular atrial septum(112, 113). The mesenchymal cells from the endocardial cushions also form the cardiac valve progenitors. Thus, disruption of endocardial EMT could explain both the valvular and septal malformation associated with PAE.

Collectively, our data on $_{HEa}$miRNAs suggest miRNA-based interventions could minimize or reverse developmental effects of PAE and other placental-related pathologies. miRNA-based therapeutic approaches have been advanced for other disease conditions. For example, Miraversen$^{tm}$, an anti-miR-122 antisense oligonucleotide, has been shown to be effective in reducing hepatitis-C viral burden (114). Additionally, a recent phase-1 clinical trial report indicated that liposomal delivery of a tumor-suppressor miRNA was well tolerated in human populations and showed evidence of therapeutic efficacy (115). However, we also observed with $_{HEa}$miRNAs that the effects of combinations of miRNAs are not a sum of their individual effects. Functional synergy between clusters of co-regulated miRNAs may be a common feature in development and disease. For instance, in 2007, we presented early evidence that ethanol exposure reduced miR-335, -21, and -153 in neural progenitors and that coordinate reduction in these miRNAs yielded net resistance to apoptosis following ethanol exposure (116). In that study, we also showed that coordinate knockdown of these three miRNAs was required to induce mRNA for Jagged-1, a ligand for the Notch cell signaling pathway, an outcome that was not recapitulated by knocking down each miRNA individually (116).

More recently, combined administration of miR-21 and miR-146a has been shown to be more effective in preserving cardiac function following myocardial infarction than administration of either of these miRNAs alone (117). While miRNA synergy has not been explored in detail, these data show that new biology may emerge with admixtures of miRNAs, and that therapeutic interventions may require the use of such miRNA admixtures rather than single miRNA molecules as have been used in

clinical studies to date. Our study was restricted to exploring the effects of the 11 $_{HEa}$miRNAs on development, which represent only the significantly increased fraction of miRNAs elevated in the HEa group maternal plasma within our Ukrainian cohort. Indeed, the next 5 most elevated miRNAs are also abundantly expressed in the placenta (data not shown), indicating they may also mediate the effects of PAE on placental biology.

# 5. CONCLUSION[*]

In conclusion, we have observed how a set of 11 miRNAs, predictive of adverse infant outcomes following PAE, collectively mediate the effects of alcohol on the placenta. Specifically, elevated levels of these miRNAs promote an aberrant maturational phenotype in trophoblasts by inhibiting core members of the EMT pathway and promoting syncytialization-dependent hormone production. Functionally, these miRNAs are clinically correlated with measures of fetal development and directly cause intrauterine growth restriction when administered *in vivo*. Our work suggests that a greater understanding for the role of $_{\text{HEa}}$miRNAs during development, and their role in coordinating the EMT pathway in the placenta and other developing tissues, will benefit the understanding of FASDs and other gestational pathologies and potentially lead to effective avenues for intervention.

[*] Part of this chapter is reprinted with permission from "Maternal circulating miRNAs that predict infant FASD outcomes influence placental maturation" by Tseng et al., 2019. *Life Science Alliance*, Vol. 2, © 2019 by Tseng et al.

# REFERENCES

1. ACOG. Committee opinion no. 496: At-risk drinking and alcohol dependence: obstetric and gynecologic implications. Obstetrics and Gynecology. 2011;118(2 Pt 1):383-8.

2. Popova S, Lange S, Probst C, Gmel G, Rehm J. Estimation of national, regional, and global prevalence of alcohol use during pregnancy and fetal alcohol syndrome: a systematic review and meta-analysis. The Lancet Global Health. 2017;5(3):e290-e9.

3. SAMHSA. The NSDUH Report: 18 percent of pregnant women drink alcohol during early pregnancy. NSDUH Report. 2013. https://www.samhsa.gov/data/sites/default/files/spot123-pregnancy-alcohol-2013/spot123-pregnancy-alcohol-2013.pdf

4. Bakhireva LN, Sharkis J, Shrestha S, Miranda-Sohrabji TJ, Williams S, Miranda RC. Prevalence of Prenatal Alcohol Exposure in the State of Texas as Assessed by Phosphatidylethanol in Newborn Dried Blood Spot Specimens. Alcohol Clin Exp Res. 2017;41(5):1004-11.

5. Riley EP, Infante MA, Warren KR. Fetal alcohol spectrum disorders: an overview. Neuropsychol Rev. 2011;21(2):73-80.

6. May PA, Gossage JP, Kalberg WO, Robinson LK, Buckley D, Manning M, et al. Prevalence and epidemiologic characteristics of FASD from various research methods with an emphasis on recent in-school studies. Developmental Disabilities Research Reviews. 2009;15(3):176-92.

7. May PA, Blankenship J, Marais AS, Gossage JP, Kalberg WO, Barnard R, et al. Approaching the prevalence of the full spectrum of fetal alcohol spectrum disorders in a South African population-based study. Alcohol Clin Exp Res. 2013;37(5):818-30.

8. Popova S, Lange S, Probst C, Gmel G, Rehm J. Estimation of national, regional, and global prevalence of alcohol use during pregnancy and fetal alcohol syndrome: a systematic review and meta-analysis. Lancet Glob Health. 2017;5(3):e290-e9.

9. Roozen S, Peters GJ, Kok G, Townend D, Nijhuis J, Curfs L. Worldwide Prevalence of Fetal Alcohol Spectrum Disorders: A Systematic Literature Review Including Meta-Analysis. Alcohol Clin Exp Res. 2016;40(1):18-32.

10. Popova S, Lange S, Burd L, Rehm J. The Economic Burden of Fetal Alcohol Spectrum Disorder in Canada in 2013. Alcohol and Alcoholism. 2016;51(3):367-75.

11. Balaraman S, Schafer JJ, Tseng AM, Wertelecki W, Yevtushok L, Zymak-Zakutnya N, et al. Plasma miRNA Profiles in Pregnant Women Predict Infant Outcomes following Prenatal Alcohol Exposure. PLoS ONE. 2016;11(11):e0165081.

12. Rossant J, Cross JC. Placental development: Lessons from mouse mutants. Nature Reviews Genetics. 2001;2:538.

13. E. Davies J, Pollheimer J, Yong HEJ, Kokkinos MI, Kalionis B, Knöfler M, et al. Epithelial-mesenchymal transition during extravillous trophoblast differentiation. Cell Adhesion & Migration. 2016;10(3):310-21.

14. Zhou Y, Damsky CH, Fisher SJ. Preeclampsia is associated with failure of human cytotrophoblasts to mimic a vascular adhesion phenotype. One cause of defective

endovascular invasion in this syndrome? The Journal of Clinical Investigation. 1997;99(9):2152-64.

15. Damsky CH, Fisher SJ. Trophoblast pseudo-vasculogenesis: faking it with endothelial adhesion receptors. Current Opinion in Cell Biology. 1998;10(5):660-6.

16. Brown LM, Lacey HA, Baker PN, Crocker IP. E-cadherin in the assessment of aberrant placental cytotrophoblast turnover in pregnancies complicated by pre-eclampsia. Histochemistry and Cell Biology. 2005;124(6):499-506.

17. Fedorova L, Gatto-Weis C, Smaili S, Khurshid N, Shapiro JI, Malhotra D, et al. Down-regulation of the transcription factor snail in the placentas of patients with preeclampsia and in a rat model of preeclampsia. Reprod Biol Endocrinol. 2012;10:15.

18. Blechschmidt K, Mylonas I, Mayr D, Schiessl B, Schulze S, Becker KF, et al. Expression of E-cadherin and its repressor snail in placental tissue of normal, preeclamptic and HELLP pregnancies. Virchows Archiv : an international journal of pathology. 2007;450(2):195-202.

19. Du L, Kuang L, He F, Tang W, Sun W, Chen D. Mesenchymal-to-epithelial transition in the placental tissues of patients with preeclampsia. Hypertension Research : Official Journal of the Japanese Society of Hypertension. 2017;40(1):67-72.

20. Gundogan F GJ, Ooi JH, Sung J, Qi W, et al. Dual Mechanisms of Ethanol-Impaired Placentation: Experimental Model. J Clin Exp Pathol. 2013:3:142. doi: 10.4172/2161-0681.1000142.

21. Tai M, Piskorski A, Kao JCW, Hess LA, M. de la Monte S, Gündoğan F. Placental Morphology in Fetal Alcohol Spectrum Disorders. Alcohol and Alcoholism. 2017;52(2):138-44.

22. Gundogan F, Gilligan J, Qi W, Chen E, Naram R, de la Monte SM. Dose effect of gestational ethanol exposure on placentation and fetal growth. Placenta. 2015;36(5):523-30.

23. Gardebjer EM, Cuffe JS, Pantaleon M, Wlodek ME, Moritz KM. Periconceptional alcohol consumption causes fetal growth restriction and increases glycogen accumulation in the late gestation rat placenta. Placenta. 2014;35(1):50-7.

24. Kalisch-Smith JI, Outhwaite JE, Simmons DG, Pantaleon M, Moritz KM. Alcohol exposure impairs trophoblast survival and alters subtype-specific gene expression in vitro. Placenta. 2016;46:87-91.

25. Bahado-Singh RO, Oz AU, Kingston JM, Shahabi S, Hsu CD, Cole L. The role of hyperglycosylated hCG in trophoblast invasion and the prediction of subsequent pre-eclampsia. Prenatal Diagnosis. 2002;22(6):478-81.

26. Muller F, Savey L, Le Fiblec B, Bussieres L, Ndayizamba G, Colau JC, et al. Maternal serum human chorionic gonadotropin level at fifteen weeks is a predictor for preeclampsia. Am J Obstet Gynecol. 1996;175(1):37-40.

27. Spencer K, Macri JN, Aitken DA, Connor JM. Free beta-hCG as first-trimester marker for fetal trisomy. Lancet (London, England). 1992;339(8807):1480.

28. Spencer K. Evaluation of an assay of the free beta-subunit of choriogonadotropin and its potential value in screening for Down's syndrome. Clin Chem. 1991;37(6):809-14.

29. Tsamou M, Vrijens K, Madhloum N, Lefebvre W, Vanpoucke C, Nawrot TS. Air pollution-induced placental epigenetic alterations in early life: a candidate miRNA approach. Epigenetics. 2018;13(2):135-46.

30. Shi Z, Zhao C, Guo X, Ding H, Cui Y, Shen R, et al. Differential expression of microRNAs in omental adipose tissue from gestational diabetes mellitus subjects reveals miR-222 as a regulator of ERalpha expression in estrogen-induced insulin resistance. Endocrinology. 2014;155(5):1982-90.

31. McAdams RM, McPherson RJ, Beyer RP, Bammler TK, Farin FM, Juul SE. Dose-dependent effects of morphine exposure on mRNA and microRNA (miR) expression in hippocampus of stressed neonatal mice. PLoS ONE. 2015;10(4):e0123047.

32. Ignacio C, Mooney SM, Middleton FA. Effects of Acute Prenatal Exposure to Ethanol on microRNA Expression are Ameliorated by Social Enrichment. Frontiers in Pediatrics. 2014;2:103.

33. Liu XD, Wu X, Yin YL, Liu YQ, Geng MM, Yang HS, et al. Effects of dietary L-arginine or N-carbamylglutamate supplementation during late gestation of sows on the miR-15b/16, miR-221/222, VEGFA and eNOS expression in umbilical vein. Amino Acids. 2012;42(6):2111-9.

34. Nemoto T, Kakinuma Y, Shibasaki T. Impaired miR449a-induced downregulation of Crhr1 expression in low-birth-weight rats. The Journal of Endocrinology. 2015;224(2):195-203.

35. Nardelli C, Granata I, Iaffaldano L, D'Argenio V, Del Monaco V, Maruotti GM, et al. miR-138/miR-222 Overexpression Characterizes the miRNome of Amniotic Mesenchymal Stem Cells in Obesity. Stem Cells and Development. 2017;26(1):4-14.

36. Baker BC, Mackie FL, Lean SC, Greenwood SL, Heazell AEP, Forbes K, et al. Placental dysfunction is associated with altered microRNA expression in pregnant women with low folate status. Molecular Nutrition & Food Research. 2017;61(8).

37. Salihu HM, Kornosky JL, Lynch O, Alio AP, August EM, Marty PJ. Impact of prenatal alcohol consumption on placenta-associated syndromes. Alcohol. 2011;45(1):73-9.

38. Khong TY. Placental vascular development and neonatal outcome. Seminars in Neonatology : SN. 2004;9(4):255-63.

39. Ray JG, Vermeulen MJ, Schull MJ, Redelmeier DA. Cardiovascular health after maternal placental syndromes (CHAMPS): population-based retrospective cohort study. Lancet (London, England). 2005;366(9499):1797-803.

40. Wang D, Na Q, Song WW, Song GY. Altered Expression of miR-518b and miR-519a in the placenta is associated with low fetal birth weight. American Journal of Perinatology. 2014;31(9):729-34.

41. Wang JM, Gu Y, Zhang Y, Yang Q, Zhang X, Yin L, et al. Deep-sequencing identification of differentially expressed miRNAs in decidua and villus of recurrent miscarriage patients. Archives of Gynecology and Obstetrics. 2016;293(5):1125-35.

42. Hromadnikova I, Kotlabova K, Ondrackova M, Pirkova P, Kestlerova A, Novotna V, et al. Expression profile of C19MC microRNAs in placental tissue in pregnancy-related complications. DNA and Cell Biology. 2015;34(6):437-57.

43. Hromadnikova I, Kotlabova K, Ivankova K, Krofta L. Expression profile of C19MC microRNAs in placental tissue of patients with preterm prelabor rupture of membranes and spontaneous preterm birth. Molecular Medicine Reports. 2017;16(4):3849-62.

44. Timofeeva AV, Gusar VA, Kan NE, Prozorovskaya KN, Karapetyan AO, Bayev OR, et al. Identification of potential early biomarkers of preeclampsia. Placenta. 2018;61:61-71.

45. Dong F, Zhang Y, Xia F, Yang Y, Xiong S, Jin L, et al. Genome-wide miRNA profiling of villus and decidua of recurrent spontaneous abortion patients. Reproduction (Cambridge, England). 2014;148(1):33-41.

46. Hu Y, Li P, Hao S, Liu L, Zhao J, Hou Y. Differential expression of microRNAs in the placentae of Chinese patients with severe pre-eclampsia. Clinical Chemistry and Laboratory Medicine. 2009;47(8):923-9.

47. Murphy MS, Casselman RC, Tayade C, Smith GN. Differential expression of plasma microRNA in preeclamptic patients at delivery and 1 year postpartum. Am J Obstet Gynecol. 2015;213(3):367.e1-9.

48. Bidarimath M, Edwards AK, Wessels JM, Khalaj K, Kridli RT, Tayade C. Distinct microRNA expression in endometrial lymphocytes, endometrium, and trophoblast during spontaneous porcine fetal loss. Journal of Reproductive Immunology. 2015;107:64-79.

49. Gao Y, She R, Wang Q, Li Y, Zhang H. Up-regulation of miR-299 suppressed the invasion and migration of HTR-8/SVneo trophoblast cells partly via targeting HDAC2 in pre-eclampsia. Biomedicine & Pharmacotherapy = Biomedecine & Pharmacotherapie. 2018;97:1222-8.

50. Sandrim VC, Luizon MR, Palei AC, Tanus-Santos JE, Cavalli RC. Circulating microRNA expression profiles in pre-eclampsia: evidence of increased miR-885-5p levels. BJOG : An International Journal of Obstetrics and Gynaecology. 2016;123(13):2120-8.

51. Rodosthenous RS, Burris HH, Sanders AP, Just AC, Dereix AE, Svensson K, et al. Second trimester extracellular microRNAs in maternal blood and fetal growth: An exploratory study. Epigenetics. 2017;12(9):804-10.

52. Martinez-Fierro ML, Garza-Veloz I, Gutierrez-Arteaga C, Delgado-Enciso I, Barbosa-Cisneros OY, Flores-Morales V, et al. Circulating levels of specific members of chromosome 19 microRNA cluster are associated with preeclampsia development. Archives of Gynecology and Obstetrics. 2018;297(2):365-71.

53. Yang S, Li H, Ge Q, Guo L, Chen F. Deregulated microRNA species in the plasma and placenta of patients with preeclampsia. Molecular Medicine Reports. 2015;12(1):527-34.

54. Hromadnikova I, Kotlabova K, Ivankova K, Krofta L. First trimester screening of circulating C19MC microRNAs and the evaluation of their potential to predict the onset of preeclampsia and IUGR. PLoS ONE. 2017;12(2):e0171756.

55. Zhang M, Muralimanoharan S, Wortman AC, Mendelson CR. Primate-specific miR-515 family members inhibit key genes in human trophoblast differentiation and are upregulated in preeclampsia. Proceedings of the National Academy of Sciences of the United States of America. 2016;113(45):E7069-E76.

56. Mei Z, Huang B, Mo Y, Fan J. An exploratory study into the role of miR-204-5p in pregnancy-induced hypertension. Experimental and Therapeutic Medicine. 2017;13(5):1711-8.

57. Choi SY, Yun J, Lee OJ, Han HS, Yeo MK, Lee MA, et al. MicroRNA expression profiles in placenta with severe preeclampsia using a PNA-based microarray. Placenta. 2013;34(9):799-804.

58. Kaufmann P, Black S, Huppertz B. Endovascular trophoblast invasion: implications for the pathogenesis of intrauterine growth retardation and preeclampsia. Biol Reprod. 2003;69(1):1-7.

59. Barrientos G, Pussetto M, Rose M, Staff AC, Blois SM, Toblli JE. Defective trophoblast invasion underlies fetal growth restriction and preeclampsia-like symptoms in the stroke-prone spontaneously hypertensive rat. Molecular Human Reproduction. 2017;23(7):509-19.

60. Roberts JM, Escudero C. The placenta in preeclampsia. Pregnancy Hypertension. 2012;2(2):72-83.

61. Fisher SJ. Why is placentation abnormal in preeclampsia? American Journal of Obstetrics and Gynecology. 2015;213(4 0):S115-S22.

62. Crosley EJ, Elliot MG, Christians JK, Crespi BJ. Placental invasion, preeclampsia risk and adaptive molecular evolution at the origin of the great apes: evidence from genome-wide analyses. Placenta. 2013;34(2):127-32.

63. Lyall F, Bulmer JN, Duffie E, Cousins F, Theriault A, Robson SC. Human Trophoblast Invasion and Spiral Artery Transformation : The Role of PECAM-1 in Normal Pregnancy, Preeclampsia, and Fetal Growth Restriction. The American Journal of Pathology. 2001;158(5):1713-21.

64. Goldman-Wohl D, Yagel S. Regulation of trophoblast invasion: from normal implantation to pre-eclampsia. Molecular and Cellular Endocrinology. 2002;187(1-2):233-8.

65. Balaraman S, Lunde ER, Sawant O, Cudd TA, Washburn SE, Miranda RC. Maternal and neonatal plasma microRNA biomarkers for fetal alcohol exposure in an ovine model. Alcohol Clin Exp Res. 2014;38(5):1390-400.

66. Panwar B, Omenn GS, Guan Y. miRmine: a database of human miRNA expression profiles. Bioinformatics. 2017;33(10):1554-60.

67. Vicovac L, Aplin JD. Epithelial-mesenchymal transition during trophoblast differentiation. Acta Anatomica. 1996;156(3):202-16.

68. Knöfler M, Pollheimer J. Human placental trophoblast invasion and differentiation: a particular focus on Wnt signaling. Frontiers in Genetics. 2013;4:190.

69. Arimoto-Ishida E, Sakata M, Sawada K, Nakayama M, Nishimoto F, Mabuchi S, et al. Up-regulation of alpha5-integrin by E-cadherin loss in hypoxia and its key role in the migration of extravillous trophoblast cells during early implantation. Endocrinology. 2009;150(9):4306-15.

70. Sun YY, Lu M, Xi XW, Qiao QQ, Chen LL, Xu XM, et al. Regulation of epithelial-mesenchymal transition by homeobox gene DLX4 in JEG-3 trophoblast cells: a role in preeclampsia. Reproductive Sciences (Thousand Oaks, Calif). 2011;18(11):1138-45.

71. Barrak J, Msheik H, Abou-Kheir W, Daoud G. Assessment of different trophoblast cell lines as in vitro models for placental development. Placenta. 2016;45:106.

72. Lovisa S, LeBleu VS, Tampe B, Sugimoto H, Vadnagara K, Carstens JL, et al. Epithelial-to-mesenchymal transition induces cell cycle arrest and parenchymal damage in renal fibrosis. Nature Medicine. 2015;21(9):998-1009.

73. Vega S, Morales AV, Ocana OH, Valdes F, Fabregat I, Nieto MA. Snail blocks the cell cycle and confers resistance to cell death. Genes & Development. 2004;18(10):1131-43.

74. Kolahi KS, Valent AM, Thornburg KL. Cytotrophoblast, Not Syncytiotrophoblast, Dominates Glycolysis and Oxidative Phosphorylation in Human Term Placenta. Scientific Reports. 2017;7:42941.

75. Lu X, He Y, Zhu C, Wang H, Chen S, Lin HY. Twist1 is involved in trophoblast syncytialization by regulating GCM1. Placenta. 2016;39:45-54.

76. Omata W, Ackerman WEIV, Vandre DD, Robinson JM. Trophoblast Cell Fusion and Differentiation Are Mediated by Both the Protein Kinase C and A Pathways. PLoS ONE. 2013;8(11):e81003.

77. Moreau R, Hamel A, Daoud G, Simoneau L, Lafond J. Expression of calcium channels along the differentiation of cultured trophoblast cells from human term placenta. Biol Reprod. 2002;67(5):1473-9.

78. Spaans F, Melgert BN, Chiang C, Borghuis T, Klok PA, de Vos P, et al. Extracellular ATP decreases trophoblast invasion, spiral artery remodeling and immune cells in the mesometrial triangle in pregnant rats. Placenta. 2014;35(8):587-95.

79. Karl PI, Chusid J, Tagoe C, Fisher SE. Ca2+ flux in human placental trophoblasts. Am J Physiol. 1997;272(6 Pt 1):C1776-80.

80. Roberts VH, Waters LH, Powell T. Purinergic receptor expression and activation in first trimester and term human placenta. Placenta. 2007;28(4):339-47.

81. Halmesmaki E, Autti I, Granstrom ML, Stenman UH, Ylikorkala O. Estradiol, estriol, progesterone, prolactin, and human chorionic gonadotropin in pregnant women with alcohol abuse. J Clin Endocrinol Metab. 1987;64(1):153-6.

82. Edelstam G, Karlsson C, Westgren M, Lowbeer C, Swahn ML. Human chorionic gonadatropin (hCG) during third trimester pregnancy. Scandinavian Journal of Clinical and Laboratory Investigation. 2007;67(5):519-25.

83. Soares MJ, Chakraborty D, Rumi MAK, Konno T, Renaud SJ. Rat Placentation: An Experimental Model For Investigating The Hemochorial Maternal-Fetal Interface. Placenta. 2012;33(4):233-43.

84. Grigsby PL. Animal Models to Study Placental Development and Function throughout Normal and Dysfunctional Human Pregnancy. Seminars in Reproductive Medicine. 2016;34(1):11-6.

85. Vercruysse L, Caluwaerts S, Luyten C, Pijnenborg R. Interstitial trophoblast invasion in the decidua and mesometrial triangle during the last third of pregnancy in the rat. Placenta. 2006;27(1):22-33.

86. Silva JF, Serakides R. Intrauterine trophoblast migration: A comparative view of humans and rodents. Cell Adhesion & Migration. 2016;10(1-2):88-110.

87. Kurtzman JT, Wilson H, Rao CV. A Proposed Role for hCG in Clinical Obstetrics. Semin Reprod Med. 2001;19(01):063-8.

88. Furcron A-E, Romero R, Mial TN, Balancio A, Panaitescu B, Hassan SS, et al. Human Chorionic Gonadotropin Has Anti-Inflammatory Effects at the Maternal-Fetal Interface and Prevents Endotoxin-Induced Preterm Birth, but Causes Dystocia and Fetal Compromise in Mice. Biology of Reproduction. 2016;94(6):136.

89. Henderson GI, Hoyumpa AM, Jr., McClain C, Schenker S. The effects of chronic and acute alcohol administration on fetal development in the rat. Alcohol Clin Exp Res. 1979;3(2):99-106.

90. O'Leary-Moore SK, Parnell SE, Godin EA, Dehart DB, Ament JJ, Khan AA, et al. Magnetic resonance microscopy-based analyses of the brains of normal and ethanol-exposed fetal mice. Birth Defects Res A Clin Mol Teratol. 2010;88(11):953-64.

91. Lo JO, Schabel MC, Roberts VH, Wang X, Lewandowski KS, Grant KA, et al. First trimester alcohol exposure alters placental perfusion and fetal oxygen availability

affecting fetal growth and development in a non-human primate model. Am J Obstet Gynecol. 2017;216(3):302.e1-.e8.

92. Bake S, Tingling JD, Miranda RC. Ethanol exposure during pregnancy persistently attenuates cranially directed blood flow in the developing fetus: evidence from ultrasound imaging in a murine second trimester equivalent model. Alcohol Clin Exp Res. 2012;36(5):748-58.

93. Gaccioli F, Lager S. Placental Nutrient Transport and Intrauterine Growth Restriction. Frontiers in Physiology. 2016;7:40.

94. Haggarty P, Abramovich DR, Page K. The effect of maternal smoking and ethanol on fatty acid transport by the human placenta. The British Journal of Nutrition. 2002;87(3):247-52.

95. Lui S, Jones RL, Robinson NJ, Greenwood SL, Aplin JD, Tower CL. Detrimental Effects of Ethanol and Its Metabolite Acetaldehyde, on First Trimester Human Placental Cell Turnover and Function. PLoS ONE. 2014;9(2):e87328.

96. Rufer ES, Tran TD, Attridge MM, Andrzejewski ME, Flentke GR, Smith SM. Adequacy of Maternal Iron Status Protects against Behavioral, Neuroanatomical, and Growth Deficits in Fetal Alcohol Spectrum Disorders. PLoS ONE. 2012;7(10):e47499.

97. Huebner SM, Blohowiak SE, Kling PJ, Smith SM. Prenatal Alcohol Exposure Alters Fetal Iron Distribution and Elevates Hepatic Hepcidin in a Rat Model of Fetal Alcohol Spectrum Disorders. The Journal of Nutrition. 2016;146(6):1180-8.

98. Xie L, Mouillet J-F, Chu T, Parks WT, Sadovsky E, Knöfler M, et al. C19MC MicroRNAs Regulate the Migration of Human Trophoblasts. Endocrinology. 2014;155(12):4975-85.

99. Salomon C, Torres MJ, Kobayashi M, Scholz-Romero K, Sobrevia L, Dobierzewska A, et al. A Gestational Profile of Placental Exosomes in Maternal Plasma and Their Effects on Endothelial Cell Migration. PLoS ONE. 2014;9(6):e98667.

100. Ouyang Y, Mouillet J-F, Coyne CB, Sadovsky Y. Placenta-specific microRNAs in exosomes – good things come in nano-packages. Placenta. 2014;35 Suppl:S69-S73.

101. Sabapatha A, Gercel-Taylor C, Taylor DD. Specific isolation of placenta-derived exosomes from the circulation of pregnant women and their immunoregulatory consequences. American Journal of Reproductive Immunology (New York, NY : 1989). 2006;56(5-6):345-55.

102. Nair S, Salomon C. Extracellular vesicles and their immunomodulatory functions in pregnancy. Seminars in Immunopathology. 2018.

103. Delorme-Axford E, Donker RB, Mouillet J-F, Chu T, Bayer A, Ouyang Y, et al. Human placental trophoblasts confer viral resistance to recipient cells. Proceedings of the National Academy of Sciences of the United States of America. 2013;110(29):12048-53.

104. Donker RB, Mouillet JF, Chu T, Hubel CA, Stolz DB, Morelli AE, et al. The expression profile of C19MC microRNAs in primary human trophoblast cells and exosomes. Molecular Human Reproduction. 2012;18(8):417-24.

105. Cronqvist T, Tannetta D, Mörgelin M, Belting M, Sargent I, Familari M, et al. Syncytiotrophoblast derived extracellular vesicles transfer functional placental miRNAs to primary human endothelial cells. Scientific Reports. 2017;7(1):4558.

106. Smith SM, Garic A, Flentke GR, Berres ME. Neural Crest Development in Fetal Alcohol Syndrome. Birth Defects Research Part C, Embryo Today : Reviews. 2014;102(3):210-20.

107. Kalcheim C. Epithelial–Mesenchymal Transitions during Neural Crest and Somite Development. Journal of Clinical Medicine. 2016;5(1):1.

108. Yang J, Qiu H, Qu P, Zhang R, Zeng L, Yan H. Prenatal Alcohol Exposure and Congenital Heart Defects: A Meta-Analysis. PLoS ONE. 2015;10(6):e0130681.

109. Burd L, Deal E, Rios R, Adickes E, Wynne J, Klug MG. Congenital heart defects and fetal alcohol spectrum disorders. Congenital Heart Disease. 2007;2(4):250-5.

110. Serrano M, Han M, Brinez P, Linask KK. Fetal alcohol syndrome: cardiac birth defects in mice and prevention with folate. Am J Obstet Gynecol. 2010;203(1):75.e7-.e15.

111. Sarmah S, Marrs JA. Complex cardiac defects after ethanol exposure during discrete cardiogenic events in zebrafish: Prevention with folic acid. Developmental Dynamics : An Official Publication of the American Association of Anatomists. 2013;242(10):1184-201.

112. Combs MD, Yutzey KE. Heart Valve Development: Regulatory networks in development and disease. Circulation Research. 2009;105(5):408-21.

113. Lin C-J, Lin C-Y, Chen C-H, Zhou B, Chang C-P. Partitioning the heart: mechanisms of cardiac septation and valve development. Development (Cambridge, England). 2012;139(18):3277-99.

114. Janssen HL, Reesink HW, Lawitz EJ, Zeuzem S, Rodriguez-Torres M, Patel K, et al. Treatment of HCV infection by targeting microRNA. The New England Journal of Medicine. 2013;368(18):1685-94.

115. Beg MS, Brenner AJ, Sachdev J, Borad M, Kang YK, Stoudemire J, et al. Phase I study of MRX34, a liposomal miR-34a mimic, administered twice weekly in patients with advanced solid tumors. Invest New Drugs. 2017;35(2):180-8.

116. Sathyan P, Golden HB, Miranda RC. Competing interactions between micro-RNAs determine neural progenitor survival and proliferation after ethanol exposure: evidence from an ex vivo model of the fetal cerebral cortical neuroepithelium. J Neurosci. 2007;27(32):8546-57.

117. Huang W, Tian SS, Hang PZ, Sun C, Guo J, Du ZM. Combination of microRNA-21 and microRNA-146a Attenuates Cardiac Dysfunction and Apoptosis During Acute Myocardial Infarction in Mice. Molecular Therapy Nucleic acids. 2016;5:e296.

118. Brady ML, Allan AM, Caldwell KK. A Limited Access Mouse Model of Prenatal Alcohol Exposure that Produces Long-Lasting Deficits in Hippocampal-Dependent Learning and Memory. Alcoholism, Clinical and Experimental Research. 2012;36(3):457-66.

119. Kajimoto K, Allan A, Cunningham LA. Fate Analysis of Adult Hippocampal Progenitors in a Murine Model of Fetal Alcohol Spectrum Disorder (FASD). PLoS ONE. 2013;8(9):e73788.

120. Watson ED, Cross JC. Development of structures and transport functions in the mouse placenta. Physiology (Bethesda). 2005;20:180-93.

121. Gårdebjer EM, Anderson ST, Pantaleon M, Wlodek ME, Moritz KM. Maternal alcohol intake around the time of conception causes glucose intolerance and insulin insensitivity in rat offspring, which is exacerbated by a postnatal high-fat diet. The FASEB Journal. 2015;29(7):2690-701.

122. Grant KA, Leng X, Green HL, Szeliga KT, Rogers LS, Gonzales SW. Drinking typography established by scheduled induction predicts chronic heavy drinking in a monkey model of ethanol self-administration. Alcohol Clin Exp Res. 2008;32(10):1824-38.

123. Carter AM. Animal models of human placentation--a review. Placenta. 2007;28 Suppl A:S41-7.

124. Orendi K, Gauster M, Moser G, Meiri H, Huppertz B. The choriocarcinoma cell line BeWo: syncytial fusion and expression of syncytium-specific proteins. Reproduction (Cambridge, England). 2010;140(5):759-66.

125. Oh SY, Hwang JR, Lee Y, Choi SJ, Kim JS, Kim JH, et al. Isolation of basal membrane proteins from BeWo cells and their expression in placentas from fetal growth-restricted pregnancies. Placenta. 2016;39:24-32.

126. Schindelin J, Arganda-Carreras I, Frise E, Kaynig V, Longair M, Pietzsch T, et al. Fiji: an open-source platform for biological-image analysis. Nature Methods. 2012;9(7):676-82.

127. Gong J, Wu Y, Zhang X, Liao Y, Sibanda VL, Liu W, et al. Comprehensive analysis of human small RNA sequencing data provides insights into expression profiles and miRNA editing. RNA Biology. 2014;11(11):1375-85.